CHALMERS
UNIVERSITY OF TECHNOLOGY

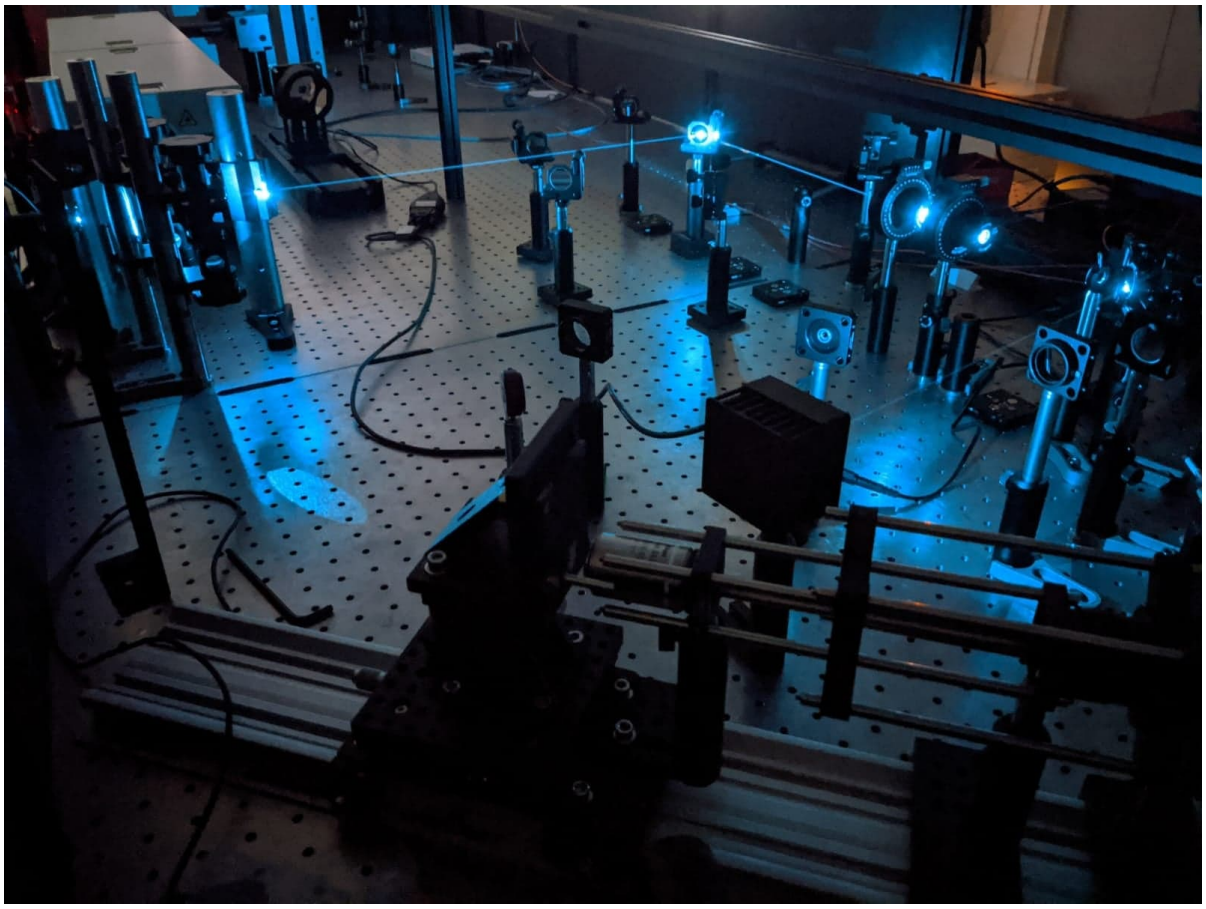

Singlet Fission - The Effects of Solvent Polarity and Conformation

Rasmus Ringström

Department of Chemistry and Chemical Engineering
Chalmers University of Technology
Gothenburg, Sweden 2022

THESIS FOR THE DEGREE OF LICENTIATE OF ENGINEERING

Singlet Fission - The Effects of Solvent Polarity and Conformation

Rasmus Ringström

Department of Chemistry and Chemical Engineering

Division of Chemistry and Biochemistry

CHALMERS UNIVERSITY OF TECHNOLOGY

Gothenburg, Sweden 2022

Singlet Fission - The Effects of Solvent Polarity and Conformation
RASMUS RINGSTRÖM

© RASMUS RINGSTRÖM, 2022

Supervisor: Bo Albinsson
Examiner: Joakim Andréasson

Licentiatuppsatser vid Institutionen för kemi och kemiteknik
Chalmers tekniska högskola
Nr 2022:11

Department of Chemistry and Chemical Engineering
Chalmers University of Technology
SE-412 96 Gothenburg
Sweden
Telephone +46 31 772 1000

Cover: Experimental setup on an optical table.

Printed by Department of Chemistry and Chemical Engineering
Gothenburg, Sweden 2022

Singlet Fission - The Effects of Solvent Polarity and Conformation

Rasmus Ringström
Department of Chemistry and Chemical Engineering
Chalmers University of Technology

Abstract

Singlet fission (SF) is a process in which one initial high energy singlet excited state is converted into two triplet excited states of roughly half the energy of the initial state. This process has the potential to increase the efficiency of conventional solar cells by modifying the energy of the incident solar radiation to better match the energy input required to generate electricity. However, the SF technology is still in an early stage of its development and a clear picture of the mechanism has not yet emerged. The aim of this thesis is to shed some light on both the mechanistic aspect and in addition investigate the integration of SF materials with semiconductors in a model system.

In the work presented herein we have demonstrated that the relative orientation of the molecules involved in the SF process governs both the rate of formation and decay of the formed triplet states in an intramolecular SF system. Transient absorption studies have revealed that it is possible to selectively excite different conformations and observe orders of magnitude different SF rates for the same molecule by changing the excitation wavelength. Furthermore, conformational changes in the excited state has been utilized to increase the lifetime of the triplet pair which could be of importance in future device implementation. Additionally, we have investigated an intermolecular SF system attached to the surface of mesoporous semiconductors. Here, we found that the surrounding solvent polarity plays a crucial part in deciding what photophysical process is favored on the surface. The study suggests that highly polar solvents are detrimental to SF and triplet injection efficiency for this system due to stabilization of charge separated states.

Keywords: Singlet fission, transient absorption, rotational conformation, photoinduced electron transfer

List of Publications

This thesis is based on the following papers:

Paper I

Molecular Rotational Conformation Controls the Rate of Singlet Fission and Triplet Decay in Pentacene Dimers. Rasmus Ringström*, Fredrik Edhborg*, Zachary W. Schroeder, Lan Chen, Michael J. Ferguson, Rik R. Tykwinski and Bo Albinsson. *Chem. Sci., 2022, 13, 4944-4954.*

Paper II

Singlet Fission and Electron Injection from the Triplet Excited State in Diphenylisobenzofuran–Semiconductor Assemblies: Effects of Solvent Polarity and Driving Force. Elin Sundin, Rasmus Ringström, Fredrik Johansson, Betül Küçüköz, Andreas Ekebergh, Victor Gray, Bo Albinsson, Jerker Mårtensson and Maria Abrahamsson. *The Journal of Physical Chemistry C, 2020, 124, 38, 20794–20805.*

My contribution to the papers

Paper I

Planned, designed and evaluated experiments together with F.E. Performed parts of the spectroscopic experiments and analyzed most of the data. Wrote most of the manuscript. DFT calculations were performed by F.E. Synthesis and related characterization were performed by Z.W.S and L.C. First authorship shared with F.E.

Paper II

Designed and performed the spectroscopic experiments and analyzed the data together with E.S. and B.K. Wrote parts of the manuscript. Synthesis and characterization were done by F.J, A.E. and V.G.

* These authors contributed equally

List of Abbreviations

CB	Conduction band
CSS	Charge separated state
DPIBF	1,3-diphenylisobenzofuran
EAS	Evolution associated spectra
ESA	Excited state absorption
ET	Electron transfer
GSB	Ground state bleach
HOMO	Highest occupied molecular orbital
IC	Internal conversion
ISC	Intersystem-crossing
IRF	Instrument response function
LUMO	Lowest unoccupied molecular orbital
OPA	Optical parametric amplifier
PET	Photoinduced electron transfer
PM	6,13-Bis(triisopropylsilylethynyl)pentacene
PMT	Photomultiplier tube
PV	Photovoltaic
S	Singlet
SAS	Species associated spectra
SF	Singlet fission
SVD	Singular value decomposition
T	Triplet
TA	Transient absorption
TCSPC	Time correlated single photon counting
VB	Valence band
VR	Vibrational relaxation

Contents

1 Introduction **1**

1.1 Purpose and Objective 4

2 Theory **5**

2.1 Light and Matter Interactions 5

2.2 Singlet Fission 13

2.3 Photoinduced Electron Transfer 16

3 Methods **21**

3.1 Steady State Absorption Spectroscopy 21

3.2 Transient Absorption Spectroscopy 22

3.3 Steady State Emission Spectroscopy 26

3.4 Time Resolved Emission Spectroscopy 27

3.5 Global Analysis of Spectroscopic Data 30

4 Results and Discussion **35**

4.1 Molecular Rotational Conformation and Singlet Fission 35

4.2 Singlet Fission and Electron Injection into Mesoporous Semiconductors 46

5 Concluding Remarks and Future Work **59**

6 Acknowledgements **61**

Bibliography **63**

1

Introduction

The world is slowly transitioning away from fossil fuel based energy resources and towards renewable alternatives. Photovoltaic (PV) devices that can convert light into electricity is an appealing option for meeting the world's energy demands and PVs currently have a central role in the transition from combustion based energy generation. PVs, often referred to as solar cells, were invented already in the early 1950s,[1] but it is only in the past two decades that the technology has seen large scale deployment and impact on the energy market. This is mainly due to a general increasing demand for renewable resources as well as a sharp decline in production costs in combination with technological advancements leading to better device performances. Since 2010 there has been an almost 70% decrease in costs of commercial PV systems and steady increase of roughly 0.3-0.4 percentage units in module efficiency every year, on average.[2] However, despite these past few years considerable increase in device efficiencies and price reduction PVs still struggle to become an economically viable option. And as with many things in today's society, short term economical gains with potential long-term disastrous consequences will in most cases be prioritized over long-term sustainable and slightly more expensive options. Consequently, it is of paramount importance to increase the efficiency and/or reduce the cost of solar cells even more to make them competitive with our current means of energy production.

The efficiency of solar energy devices is however fundamentally limited due to the so-called spectrum losses which stems from a mismatch between the photon energies in the solar spectrum and the energy input required for the solar cells. The mismatch originates from the fact that semiconductors, which is the material that conventional solar cells are made of, have a fixed band gap. Band

gap refers to the minimum energy an incident photon must have to be absorbed and to generate an electron-hole pair which in turn is a necessary requirement to generate electricity if the semiconductor is connected to an electrical circuit. Figure 1.1 presents the solar spectrum together with the band gap of silicon (1.1 eV)[3] which is the semiconductor that the vast majority of commercial solar cells today are made of.[4] Photons with an energy that exceeds the band gap, i.e. photons with wavelengths shorter than roughly 1150 nm, have an excess of energy relative to the band gap of silicon. Photons from this part of the spectra can still only generate a single electron-hole pair and the excess energy is lost as heat. The losses associated with this energy excess are the dominant losses of single junction silicon solar cells and are referred to as thermalisation losses (single junction refers to a solar cell containing only a single type of semiconductor with a specific band gap). The thermalisation losses combined with the losses associated with photons that have too low energy to be absorbed at all results in an upper theoretical efficiency limit called the Shockley-Queisser limit. It is named after William Shockley and Hans J. Queisser whom in 1961 calculated the thermodynamic energy conversion limit of any single junction cell to approximately 33 %.[5]

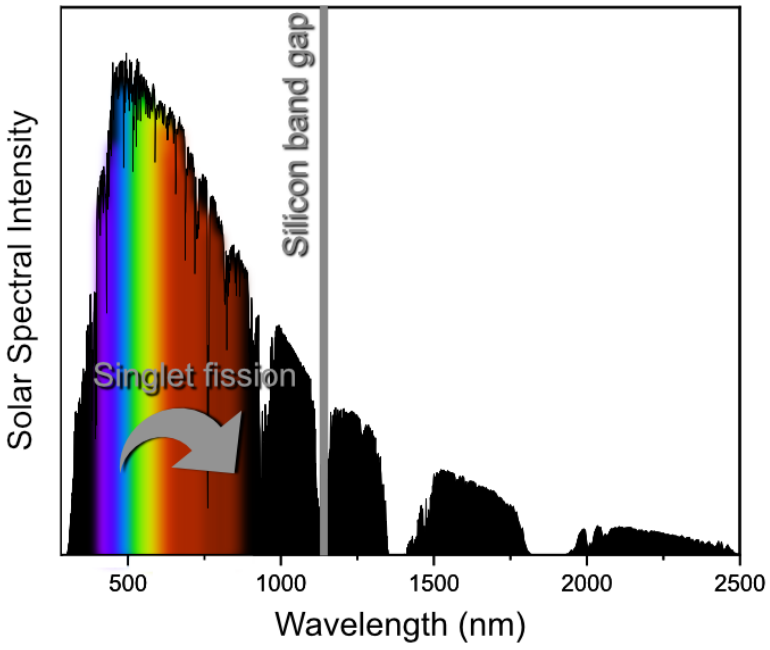

Figure 1.1: The solar spectrum at sea level plotted together with the band gap of silicon and an arrow indicating how singlet fission can be used to increase the efficiency of photovoltaic devices. Data was obtained from National Renewable Energy Laboratory.[6]

Several technologies are currently being investigated to increase the efficiency of solar cells beyond the Shockley-Queisser limit. The technique relevant to this thesis is a photon energy conversion technique that aims to change the energy of the incoming photons from the Sun so that they match better with the band gap of solar cells. The technique is called singlet fission (SF) and it is a multiple exciton generation process. The process is initiated by absorption of a photon by a molecule raising it to a temporary excited state. While in this excited state it can share its energy with a neighbouring molecule resulting in both molecules ending up in excited states of roughly half the energy of the initially excited state.[7] If both of these lower energy excited states have enough energy to create one electron-hole pair each in the semiconductor the thermalisation losses are partially overcome. In total, SF has the potential to increase the Shockley-Queisser limit from ~33 % to ~41 %.[8,9] This may at first appear to be a very modest increase. However, an increase of only a few percentage units can still have a large impact considering the abundance of sunlight that is received by the Earth every day. The amount of energy from the Sun that reaches the Earth in just a few hours is estimated to be equal to the global energy consumption of a full year.[10] Furthermore, the SF material could in principle be integrated directly with existing solar cells as an extra layer as illustrated in Figure 1.2 and would thus not require extensive engineering in an ideal scenario.

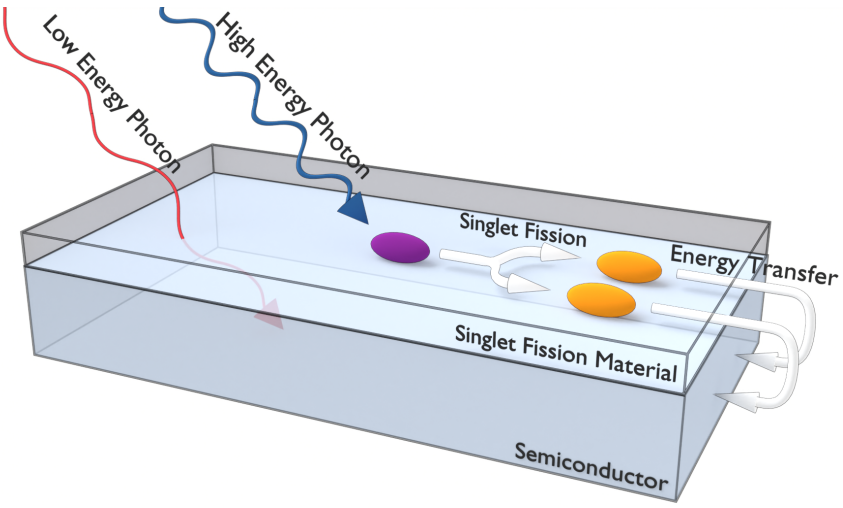

Figure 1.2: Illustration of the theoretical implementation of SF in a PV device. Low energy photons are used without energy alteration whereas high energy photons are absorbed by the SF material and converted to two energy states of lower energy.

1.1 Purpose and Objective

Although SF is a promising technology for overcoming thermalisation losses in solar cells, the technology is in its current state not ready for application in commercial systems. The aim of this thesis is to acquire more knowledge about the mechanism of SF, which is still not well understood, with the ultimate goal of understanding how it best can be applied in future devices. In both of the papers presented in this thesis, derivatives of two well known SF molecules have been investigated, but with slightly different focus.

In **Paper I** a dimer of 6,13-Bis(triisopropylsilylethynyl)pentacene (PM) has been investigated with emphasis on the role of molecular orientation of the two moieties that undergo SF relative to each other. Dimers are interesting to study from a mechanistic perspective since they allow precise control of mainly distance but also to some degree orientation and electronic coupling between the SF moieties. This is in stark contrast to individual monomers in solution where the molecules can come into contact in a more or less infinite number of configurations. However, even dimeric structures are not fully static systems and this study thus also sought to understand how dynamics in the excited state governs the rate of SF and the subsequent lifetime of the formed excited states. This is an often overlooked parameter in the literature.

In **Paper II** a derivative of 1,3-diphenylisobenzofuran (DPIBF) was attached to different semiconductors and the ability of the excited states of DPIBF subsequent to the SF event to create electron-hole pairs in the semiconductors was evaluated. The study involved several different semiconductors and various solvents to investigate if driving force and environment can be used to control which photophysical process is favored on the surface.

2

Theory

Spectroscopy, which is a central part of solar cell and SF research, is the study of absorption, emission and scattering of electromagnetic radiation by atoms or molecules. The tool with which we explain and understand light and matter interactions at this fundamental level is quantum mechanics. The theory of quantum mechanics was slowly developing towards the end of the 19th century and the beginning of the next century as physicists were trying to understand and explain experimental observations such as the photoelectric effect. Years of effort from renowned scientists such as Planck, Einstein and de Broglie culminated in the formulation of quantum mechanics by both Schrödinger and Heisenberg in 1927.[11] The theories that emerged have since then been built upon and are still highly relevant across all of physics and photochemistry today. The aim of this chapter is to introduce the most central photophysical concepts relevant to the contents of this thesis and explain them with the help of some of the quantum mechanical theories that were developed almost 100 years ago.

2.1 Light and Matter Interactions

Photochemistry is a branch of chemistry that is concerned with the interaction of electromagnetic radiation, i.e. light, with matter. Light can be described as an electric field that oscillates perpendicularly to an oscillating magnetic fields as illustrated in Figure 2.1. The two fields propagate in the same direction and the distance between two maxima on either field is called the wavelength (λ). The SI unit of wavelength is metres (m) but it is often expressed in nanometers (10^{-9}m, nm) for the purpose of electronic spectroscopy.[12]

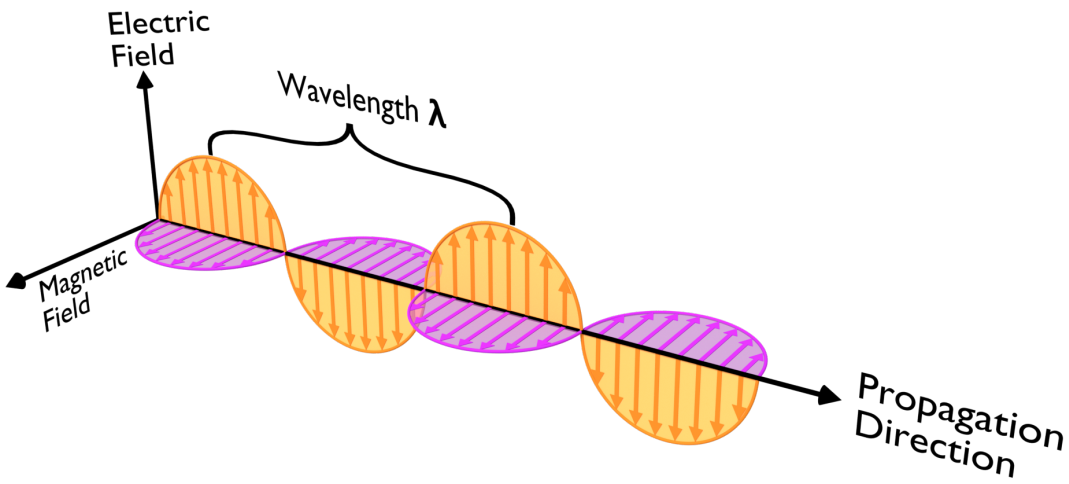

Figure 2.1: Illustration of the propagation of an electromagnetic wave with perpendicularly oscillating electric and magnetic fields.

It is however often convenient to describe light not only as a wave, but also as particles referred to as photons. The energy of photons (E_{photon}) is related to the wavelength, or frequency (ν), of the oscillating electric and magnetic field together with Planck's constant (h, 6.62607015·10^{-34} Js^{-1}) and the speed of light in vacuum (c, 299 792 458 m s^{-1}) according to equation 2.1.[13]

$$E_{photon} = \frac{hc}{\lambda} \tag{2.1}$$

In order to understand how and in what ways light can interact with matter we must also briefly describe the nature of matter itself. The smallest constituents of matter that will be considered for the contents of this thesis are protons, neutrons and electrons that together form atoms. Atoms are in turn the basis of molecules and larger everyday objects and materials around us. As it turns out, matter on the macroscopic level can, just as photons, be described as both waves and as particles. This is known as the wave-particle duality. The negatively charged electrons are distributed in space around the nuclei consisting of the positively charged protons and neutral neutrons. A consequence of the small size of electrons and atoms in general is that their energy is restricted to discrete states and values. The energy is said to be quantized and for atoms and molecules this means that the electrons are restricted to different orbitals of

certain energies. The energies (E) of the orbitals are given by the solution to the Schrödinger equation as shown in equation 2.2

$$\hat{H}\,\psi = E\,\psi \tag{2.2}$$

where ψ is the electronic wavefunction which describes the motion and location of electrons around the nuclei which is also found by solving the equation. $\hat{H}$ is the Hamiltonian operator that describes the total energy of the system. According to Pauli's exclusion principle both atomic orbitals (AO) and molecular orbitals (MO, which are formed by linear combination of AOs) can be occupied by a maximum of two electrons, and if two electrons do occupy one orbital, their spins must be paired. Here, spin refers to the intrinsic quantum mechanical property of electrons. It is easy to envision spin as an actual spinning motion of the electron, but this classical mechanical viewpoint of a quantum mechanical property is not entirely correct and it is better to think about spin just as any property of electrons such as charge or rest mass. Spin is nonetheless important and electrons can have a spin of either +1/2 (up) or -1/2 (down). Two electrons that share an orbital will thus have opposite spins as illustrated in Figure 2.2 where the electrons are symbolized as half arrows pointing up or down in orbitals represented as lines.[11]

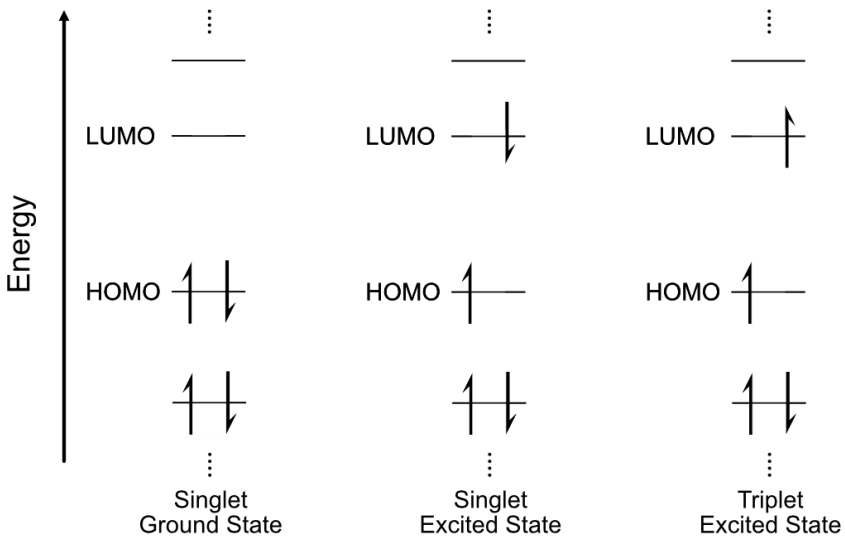

Figure 2.2: Orbital energy diagram with electrons symbolized as half-arrows illustrating the different spin multiplicity states of singlet and triplet.

Figure 2.2 further shows that electrons occupy lower energy orbitals before filling higher energy ones according to the Aufbau principle (from the german word for building up). The highest occupied molecular orbital (HOMO) and lowest unoccupied molecular orbital (LUMO) are of considerable interest to photochemists because even if there are a multitude of filled molecular orbitals lower in energy, most photophysical properties in molecules are based on these frontier orbital electrons that are more energetically accessible. As indicated in Figure 2.2 an electron is in a so called singlet ground state when the HOMO is filled with two electrons forming a closed shell with net zero spin (one up and one down). Here, ground state refers the lowest energy electronic configuration of the molecule and the word singlet refers to the spin multiplicity of the molecule. A two electron system can have a spin multiplicity of one or three where one indicates that it is a singlet state with anti-parallel spin and three means that it is a triplet state with parallel spin. Figure 2.2 also shows two other electron configurations called singlet excited state and triplet excited state. An electronically excited state can be formed if a molecule or atom absorbs energy, for instance in the form of a photon. This may raise the molecule to a temporary higher energy state by moving an electron from a lower energy to a higher energy orbital. This can occur if the incoming photon energy matches the energy gap (ΔE) between the initial and final state and is known as Bohr's frequency condition.[12,14]

$$\Delta E = E_{photon} = \frac{hc}{\lambda} = h\nu \tag{2.3}$$

In the excited state the two electrons are separated in different orbitals and consequently, Pauli's exclusion principle no longer demands that the two electrons have paired spin. As a result, an initial singlet ground state (which the vast majority of organic molecules are in) can have a different spin multiplicity in the excited state. However, there are also some molecules that have a triplet ground state. One such example is molecular oxygen (O_2) which has two degenerate (same energy) highest lying orbitals each occupied by one electron that allows for parallel spins of the electron pair even in the ground state.[15]

Once formed, excited states are inherently energetically unstable and atoms and molecules will decay back to the ground state after a certain time period that is highly system dependent. The processes that can occur subsequent to absorption of a photon are commonly depicted in a Jablonski diagram such as the one in Figure 2.3. Here, electronic levels are represented as solid thick horizontal lines and the singlet ground state is denoted as S_0. The first singlet excited state is denoted as S_1 and so on for higher energy excited states whereas triplet excited states are denoted as T_n. The electronic levels all contain numerous vibrational and rotational energy levels spaced between them. The vibrational levels are shown as horizontal thin solid lines and are separated by energies that range from approximately 0.1 to 0.15 eV which in wavelength scale is around 8-10 μm. This can be compared to the energy spacing between electronic energy levels which, for a typical organic molecule, is on the order of 1.5 to 3.5 eV corresponding to transitions in the ultraviolet-visible region (UV-vis, 350-750 nm). The energy separating the rotational energy levels are almost two orders of magnitude smaller than the energy separation of vibrational energy levels and have thus been omitted in the diagram for visual clarity.[16]

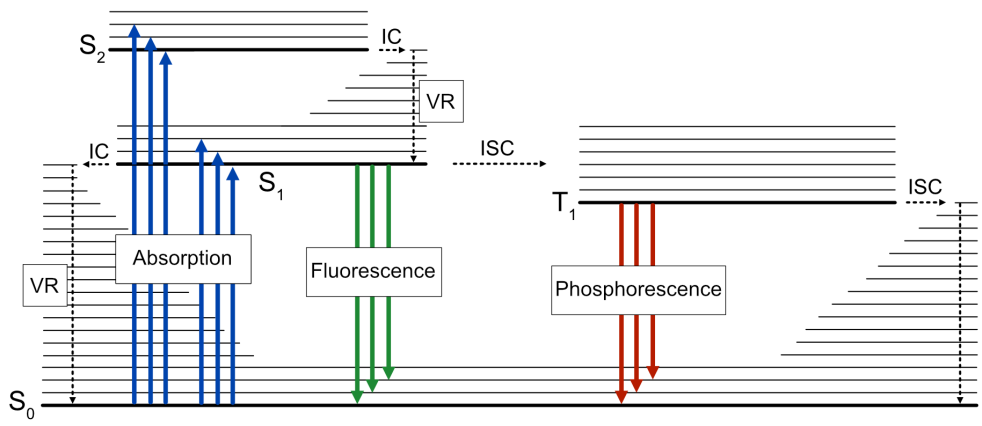

Figure 2.3: Jablonski diagram with singlet (S) and triplet (T) energy levels shown as horizontal lines. Thick lines depict the electronic levels and thinner horizontal lines are the vibrational levels. The diagram illustrates a selection of common photophysical processes such as absorption, fluorescence, phosphorescence, internal conversion (IC), vibrational relaxation (VR) and intersystem-crossing (ISC). Photoexcitation and radiative decay processes are marked as solid lines and non-radiative processes are marked as dotted lines.

Photoexcitation occurs from the ground state S_0 to excited states of the same multiplicity S_n. Transitions directly to triplet states T_n are *spin forbidden* since a change of spin in conjunction with a transition is not allowed. However, as will be described shortly, even "forbidden" processes can in fact sometimes still occur, albeit with very low probability. From the excited singlet state S_n the molecule will quickly relax to different electronic levels of the same multiplicity via internal conversion (IC) and via vibrational relaxation (VR) to different vibrational levels. These non-radiative processes are marked as dotted arrows in the Jablonski diagram. IC and VR can occur on the sub picosecond (10^{-12} s) time scale between states where the energy difference is small such as for transitions from S_n to S_1 (or from T_n to T_1). As a result, most photophysical processes in solution occur predominantly from S_1 or T_1 since these states are generally more long-lived. This is known as Kasha's rule.[17] From S_1 the molecule can return to the ground state via radiative or non-radiative processes that typically occur on the nanosecond time scale (10^{-9} s). The non-radiative processes involve internal conversion and vibrational relaxation just as for higher excited states. The radiative relaxation from S_1 to S_0 is called fluorescence and involves the emission of a photon with an energy that is determined by the energy gap between the two energy levels. S_1 can also decay non-radiatively to a triplet state T_n in a process called intersystem crossing (ISC). As mentioned previously, a transition involving a spin change is quantum mechanically forbidden and consequently this process typically occurs slowly due to its low probability. The rate can however vary from the microsecond (10^{-6} s) to the picosecond timescale since it can be heavily influenced by the magnitude of spin-orbit coupling in the molecule. Spin-orbit coupling refers to the interaction between the spin of the electrons and the orbital motion of the electrons around the nucleus. The magnitude of spin-orbit coupling is related to the nuclear charge and is larger for molecules containing heavy atoms. This is called the heavy atom effect and it is known to enhance the rate of spin-forbidden processes such as ISC.[14]

Note that in the processes described above intermolecular relaxation pathways such as energy and electron transfer are not included. Electron transfer will be described in more detail in section 2.3 and regarding non-radiative energy transfer there are two main mechanisms: Dexter energy transfer[18] and Förster

resonance energy transfer (FRET).[19] Dexter energy transfer is a short-range (few Å , 10^{-10} m) energy transfer mechanism involving a virtual electron exchange between a donor and an acceptor molecule. FRET on the other hand can occur over longer distances (few nm) and is dependent on the spectral overlap of the donor emission and acceptor absorption.

It should be mentioned that transitions between different electronic states often involve a combination of vibrational and rotational levels which results in broadening of absorption and emission spectra since most detectors cannot accurately resolve each individual transition when they are too closely spaced in terms of energy. This is the main reason why measured absorption and emission spectra in solution are typically not observed as discrete lines as Bohr's frequency condition in equation 2.3 would suggest. Two typical absorption and emission spectra are presented in Figure 2.4.

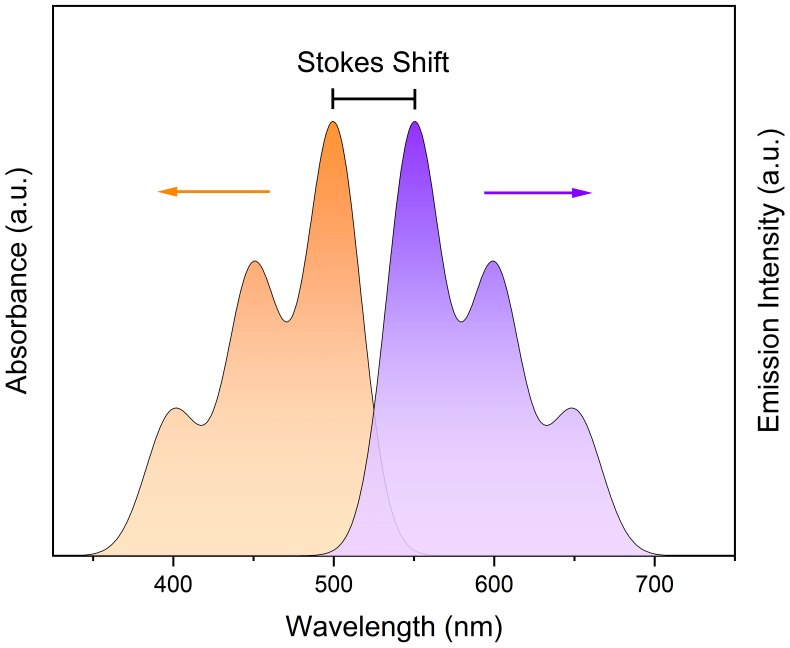

Figure 2.4: Absorption and emission spectra of a hypothetical molecule. The emission spectrum is a mirror image of the absorption spectra and the emission is shifted to longer wavelengths compared to the absorption.

Both the absorption and emission spectra have a clear vibronic progession with

transitions from or to different vibrational levels within the electronic levels. The emission is often found to be a mirror image of the absorption spectra as illustrated here because of the previously mentioned Kasha's rule resulting in emission being mainly from S_1 to different vibrational levels of S_0. Analogous, absorption transitions occur from the ground state to different vibrational levels in S_1 and the similarity in spectra originates from the fact that the energy spacing is similar for the vibrational levels of S_0 and S_1. Figure 2.4 also indicates the characteristic Stokes shift of the emission relative to the absorption which is a result of the non-radiative relaxation processes that occurs in between the absorption and emission events.[20] Additional reasons for line broadening in the gas phase include phenomena such as natural linewidth broadening due to the Heisenberg uncertainty principle and doppler broadening where the absorbed or emitted frequency depends on the velocity of the molecule or atom relative to the detector. Spectra can also be broadened, change shape or shift in wavelength when the surrounding environment is altered. One common reason for this, which will be seen in both Paper I and II, is that different solvents can stabilize the formed excited states to different extents following absorption of a photon. For instance, an excitation may result in a more polar molecule in the excited state compared to the ground state due to the fact that an electron subsequent to excitation may occupy an orbital located on a different part of the molecule. A more polar excited state is stabilized in a more polar solvent environment which in this scenario would result in a red-shift of the absorption spectra.

2.1.1 Quantum Yield and Excited State Lifetime

Spectroscopists use several different parameters to characterize and quantify processes that occur in systems under investigation. One frequently encountered and important parameter when dealing with photophysical processes is quantum yield (ϕ). Quantum yield is defined as the number of events that occur per photon absorbed in a given system according to equation 2.4.

$$\phi = \frac{\#events}{\#absorbed\ photons} \tag{2.4}$$

The quantum yield can refer to any photoinduced process such as fluorescence (ϕ_f), intersystem crossing (ISC) (ϕ_{ISC}) or even SF (ϕ_{SF}). It is also possible to

express quantum yields in terms of the rate constant of the process in question (k_i) divided by the sum of all the rate constants (k_j) that can deactivate the state according to equation 2.5.

$$\phi = \frac{k_i}{\sum_j k_j} \tag{2.5}$$

In the case of for instance fluorescence, k_i would be the radiative relaxation rate constant (k_r) and the sum of k_r and the rate constant of all non-radiative processes (k_{nr}) would be placed in the denominator as shown in equation 2.6.

$$\phi_f = \frac{k_r}{k_r + k_{nr}} \tag{2.6}$$

The inverse sum of all the rate constants, i.e. the denominator in equation 2.5 and 2.6, is another important parameter called the lifetime (τ) of a state. The lifetime is thus inversely proportional to all rate constants that depopulate the state as described in equation 2.7 and is the average time a molecule spends in its excited state. Lifetimes and methods to experimentally determine them will be explained in more detail in section 3.4 and 3.5.

$$\tau = \frac{1}{\sum_j k_j} \tag{2.7}$$

2.2 Singlet Fission

Singlet fission (SF) is a multiple exciton generation process where one initial excited singlet state molecule shares its excitation energy with a ground state molecule. The result is the formation of two triplet excited states where the formed triplets are initially strongly coupled in a correlated triplet pair $^1(T_1T_1)$ with an overall singlet spin multiplicity.[7,21] Since the product of SF are two triplet excited states for each absorbed photon the maximum quantum yield, as defined in equation 2.4, is 200 %. Figure 2.5 shows a simplified mechanistic scheme of SF where the process is initiated by photoexcitation of one molecule to its first singlet excited state.

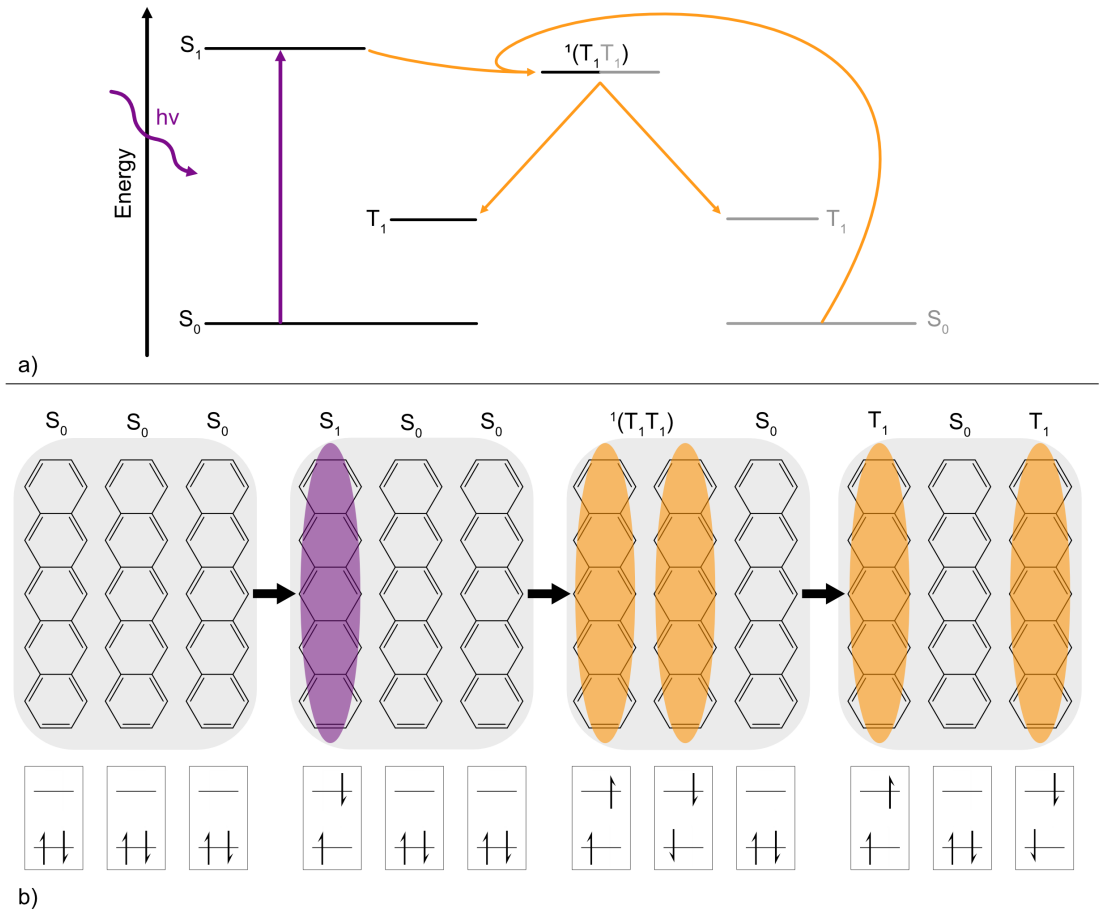

Figure 2.5: a) Jablonksi diagram of the SF process starting with the exitation of a single molecule followed by formation of the correlated triplet pair and finally independent triplet states. b) Schematic of the SF process with pentacene as a model SF molecule. The arrows indicate the spin of the involved states.

Because of the singlet spin multiplicity of the correlated triplet pair the initial step of SF is spin allowed and may occur on the sub picosecond timescale and can in certain cases even outcompete IC and VR. As previously mentioned, and as indicated in the Jablonski diagram, the final step of SF involves decorrelation and separation of the triplet pair into two fully independent triplet states. This process typically requires spatial separation of the triplets as shown in Figure 2.5b. It should be noted that the kinetic scheme of SF is often more complicated than the one presented in Figure 2.5 due to the involvement intermediate states such as excimers,[22] charge transfer states[23] or triplet-pair species with different spin multiplicities.[24] The scheme presented is thus just the general process and the actual mechanism is most aptly described as system dependent since it

has been proven occur by different mechanism for different SF capable classes of molecules or even different assemblies and geometries of the same type of molecule.[25–27]

Even though SF can occur efficiently on ultrafast timescales the process as depicted in Figure 2.5a is typically not represented in a general Jablonski diagram such as the one in Figure 2.3. There are in principle two main reasons for this. The first has its origin in the fact that SF requires two molecules in close proximity or at least two sites that can each accommodate a triplet exciton and is thus not a general process for a typical single organic molecule in solution. Secondly, there are relatively few classes of molecules that fulfils the energetic requirements needed to undergo SF. For SF to occur the energy of the lowest singlet excited state $E(S_1)$ must exceed twice the energy of the lowest excited triplet state $E(2T_1)$. This thermodynamic condition is typically not satisfied for organic molecules. SF can however be slightly endothermic or occur from a vibrationally excited S_1, but must then compete with vibrational relaxation. Despite the mentioned requirements, SF has been observed and confirmed in a number of different molecules. Examples include linear polyacenes such as tetracene[28–30] and pentacene[31,32] and other molecular classes such as 1,3-diphenylisobenzofuran,[33–35] rylenes[36,37] and derivatives thereof. Due to the requirement of short distance between the SF molecules, SF has been extensively studied in crystals where the molecules are neatly packed and organized. However, SF has also been investigated in highly concentrated solutions.[22,38,39] This is another example of intermolecular SF, albeit with less control of order and orientation of the molecules involved in the SF process. A third method of satisfying the distance dependence is to design systems in which intramolecular SF can take place by for instance covalently linking two or more SF capable molecules to each other. Molecules consisting of two, three or more linked molecules are often referred to as dimers, trimers etc. Contrary to intermolecular SF where the triplet excitons can decorrelate and diffuse apart leading to long triplet lifetimes, intramolecular SF often suffers from short triplet-pair lifetimes. This is mainly because the inability of the triplet-pair to diffuse apart which in turn may lead to triplet recombination due to the strong electronic coupling between the molecules that is often present in for instance a dimer. The design

of a SF dimer is thus all about having strong enough electronic coupling for SF to occur efficiently and outcompete other processes such as fluorescence or IC while simultaneously making sure that the coupling is not so strong that the triplet-pair is deactivated immediately after being formed. This is important to consider since the triplets have to be formed quantitatively and at the same time have long lifetimes to be useful in any future application.

As evident from the above description of SF, the final product are two (generally) non-emissive triplet states. Thus, in order to actually utilize SF as a method to increase the efficiency of solar cells a final step has to be included that is concerned with the harvesting of the generated excitons. This could for instance be achieved by energy transfer from the individual triplets to an emissive specie that can emit photons which in turn may be absorbed by the solar cell material. Another possibility is to utilize the triplet energy directly in a process called photoinduced electron transfer where each triplet state resulting from SF injects one electron into the semiconductor that the solar cell is made of. Photoinduced electron transfer and electron transfer in general will be described in more detail in the following section.

2.3 Photoinduced Electron Transfer

Electron transfer (ET) reactions can be described as events where electrons are transferred from a donor (D) to an acceptor (A). ET can occur both when the donor or acceptor are in their respective ground states or excited states. In both cases, ET only occurs if there is a driving force for the reaction.[40,41] When ET occurs to or from an excited state that has been temporarily formed *via* absorption of a photon the process is called photoinduced electron transfer (PET).[42] It is generally easier to oxidize (remove an electron) from an excited state molecule than it is from the ground state since the excitation energy (singlet- or triplet excited state energy) counts towards the total energy needed to remove the electron completely from the molecule. Conversely, it is also easier for a specie to be reduced (accept an electron) if it is in an excited state since the addition of an electron may occupy the now half vacant HOMO orbital (in the case of a closed shell molecule). Consequently, in both cases the driving force for ET is

typically increased by first exciting either the donor or acceptor. The rate of an ET event can be estimated using Marcus theory and the rate constant k_{ET} can be expressed according to equation 2.8.[43,44]

$$k_{ET} = \kappa_{el}\nu_n e^{-\frac{(\lambda+\Delta G^0)^2}{4\lambda k_B T}} \tag{2.8}$$

Here, κ_{el} is the electronic transmission coefficient, ν_n is related to the nuclear motion, k_B is Boltzmann's constant and T is the temperature. The energy barrier ΔG^0 can also be seen as the driving force for the reaction and, finally, λ is the reorganization energy related to the rearrangement of the donor and acceptor and the surrounding solvent molecules. From the equation it is possible to deduce a somewhat surprising result which is that as the driving force increases, i.e., when ΔG^0 becomes more negative, the rate of electron transfer will only increase so long as $-\Delta G^0 < \lambda$. If $-\Delta G^0 > \lambda$ the rate of electron transfer decreases with increasing driving force. This is a well-known and confirmed phenomena in the field of ET and if it is observed the ET is referred to as being in the inverted region.[45] In addition to the rate constant of ET it is sometimes useful to estimate how likely a particular ET event is based on the driving force of creating the charge separated state (CSS) of the donor and acceptor $\Delta G(D^{\cdot+} - A^{\cdot-})$ in accordance with the Marcus-Rehm-Weller in equation 2.9.[46,47] A negative value of $\Delta G(D^{\cdot+} - A^{\cdot-})$ means that the ET for a particular reaction is spontaneous.

$$\Delta G(D^{\cdot+} - A^{\cdot-}) = E_{ox}(D) - E_{red}(A) - \frac{e^2}{4\pi\epsilon_0\epsilon_s R_{DA}} - \Delta E_{00} \tag{2.9}$$

Here, $E_{ox}(D)$ is the oxidation potential of the donor, $E_{red}(A)$ is the reduction potential of the acceptor. The next term is the related to the coulombic stabilization effects associated with bringing the two charges close to one another. ϵ_0 is the permeability of vacuum ($8.854 \cdot 10^{-12}$ As/Vm), ϵ_s is the relative dielectric constant of the solvent and R_{DA} is the center-to-center distance between the donor and acceptor. ΔE_{00} is the excited state energy of the donor which highlights the importance of PET since it may render normally nonspontaneous ET reactions spontaneous.

2.3.1 Semiconductors

A semiconductor is a solid phase material consisting of a large number of atoms that is characterized by the fact that it has two distinct energy bands rather than several distinct energy levels such as those for an atom or molecule.[48] The origin of the band structure can be understood by considering what happens when a large number of atoms come together to form a solid. In this scenario, each atom provides their own orbitals that, when combined, will slightly shift in energy from the original value that they had when the atoms existed in isolation. As more and more atoms congregate the number of energy levels will increase and the separation between them becomes finer until there in principle is a continuum of energy levels that ultimately forms two energy bands. For a semiconductor the low energy band which is fully occupied with electrons is referred to as valance band (VB) and the upper energy band is called the conduction band (CB). Figure 2.6 presents a schematic illustration that shows the difference between semiconductor energy bands and the discrete energy levels of a molecule or atom.

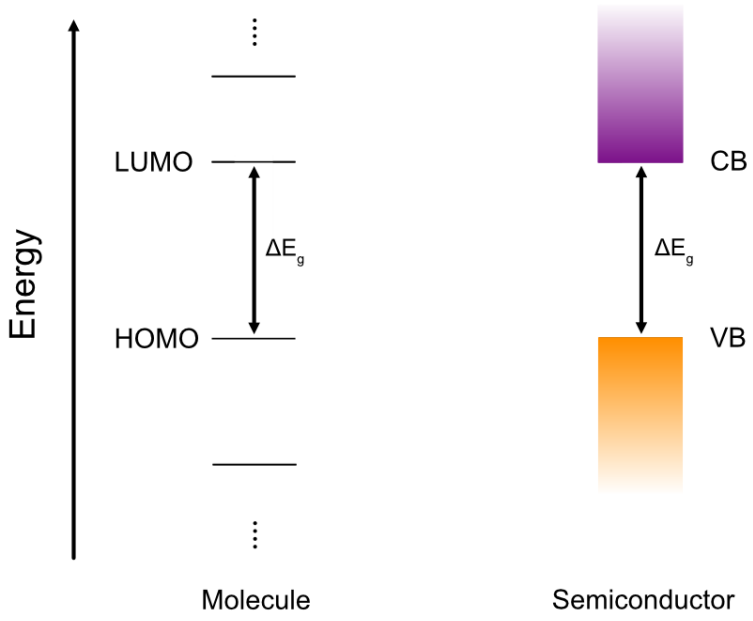

Figure 2.6: Illustration of the energy level distribution in a molecule compared to a semiconductor material.

For a semiconductor the CB contain no electrons at 0 K and is separated from the VB by the band gap E_g, which corresponds to the energy required to promote an electron from the VB to the CB. The promotion can for instance occur by absorption of a photon with energy that exceeds the band gap. The conduction band can however also be populated by accepting an electron from another molecule i.e. via PET. When a semiconductor is an acceptor in a PET reaction the ET event is commonly referred to as electron injection.

3

Methods

This section presents and explains the spectroscopic techniques and fitting procedures used in this work.

3.1 Steady State Absorption Spectroscopy

Steady state absorption spectroscopy can be used to assess what type of substance a sample contains and it can also be used to quantify the concentration of a substance present in the sample. Figure 3.1 shows the main components of an absorption spectrometer.

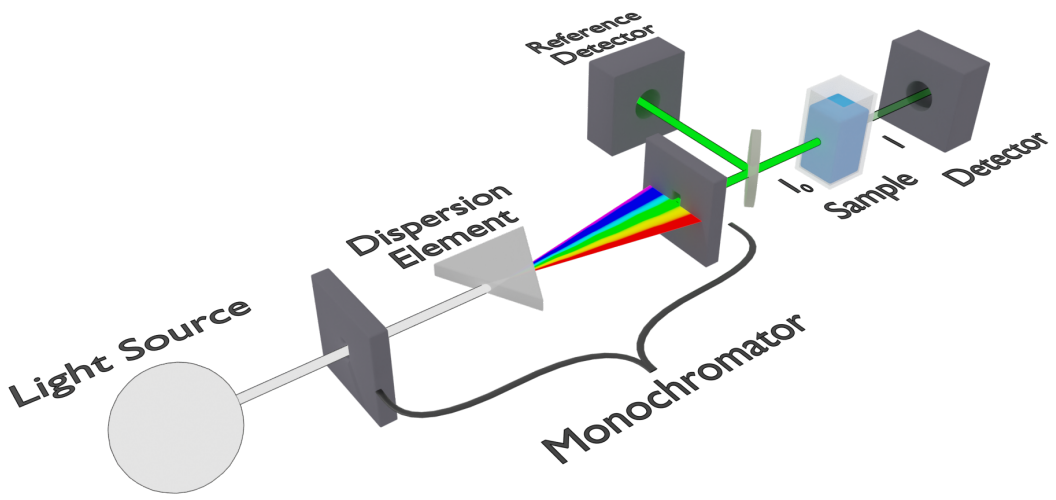

Figure 3.1: Schematic illustration of an absorption spectrometer.

The monochromator consists of a dispersive element, usually a diffraction grating, that spreads the light in different angles as a function of the wavelength, and a thin slit which is used to select the desired wavelength. The intensity be-

fore the sample (I_0) is measured by a reference detector and the intensity of the light having passed through the sample (I) is measured by a separate detector. The absorbance (A) can then be calculated according to equation 3.1.[12]

$$A = \log \frac{I_0}{I} \tag{3.1}$$

The absorbance of a sample is proportional to the concentration (C), the path-length (l) and the molar absorptivity at a particular wavelength ($\epsilon(\lambda)$) according to equation 3.2.

$$A(\lambda) = \epsilon(\lambda) C l \tag{3.2}$$

The molar absorptivity is a measure of the probability for a molecule or a material to absorb a photon of a certain wavelength.[13]

3.2 Transient Absorption Spectroscopy

Whereas steady state absorption generally provides an absorption spectrum of the ground state, transient absorption (TA) spectroscopy can be used to probe the absorption of transient species such as excited states. TA is often referred to as pump-probe spectroscopy and the basic principle of this technique is that the sample is initially excited by an intense pulse (pump) that populates the excited states. The pump pulse is followed by a weaker pulse (probe) after a certain time delay. The purpose of the probe pulse is to measure the absorption induced by the first pulse as illustrated in Figure 3.2.

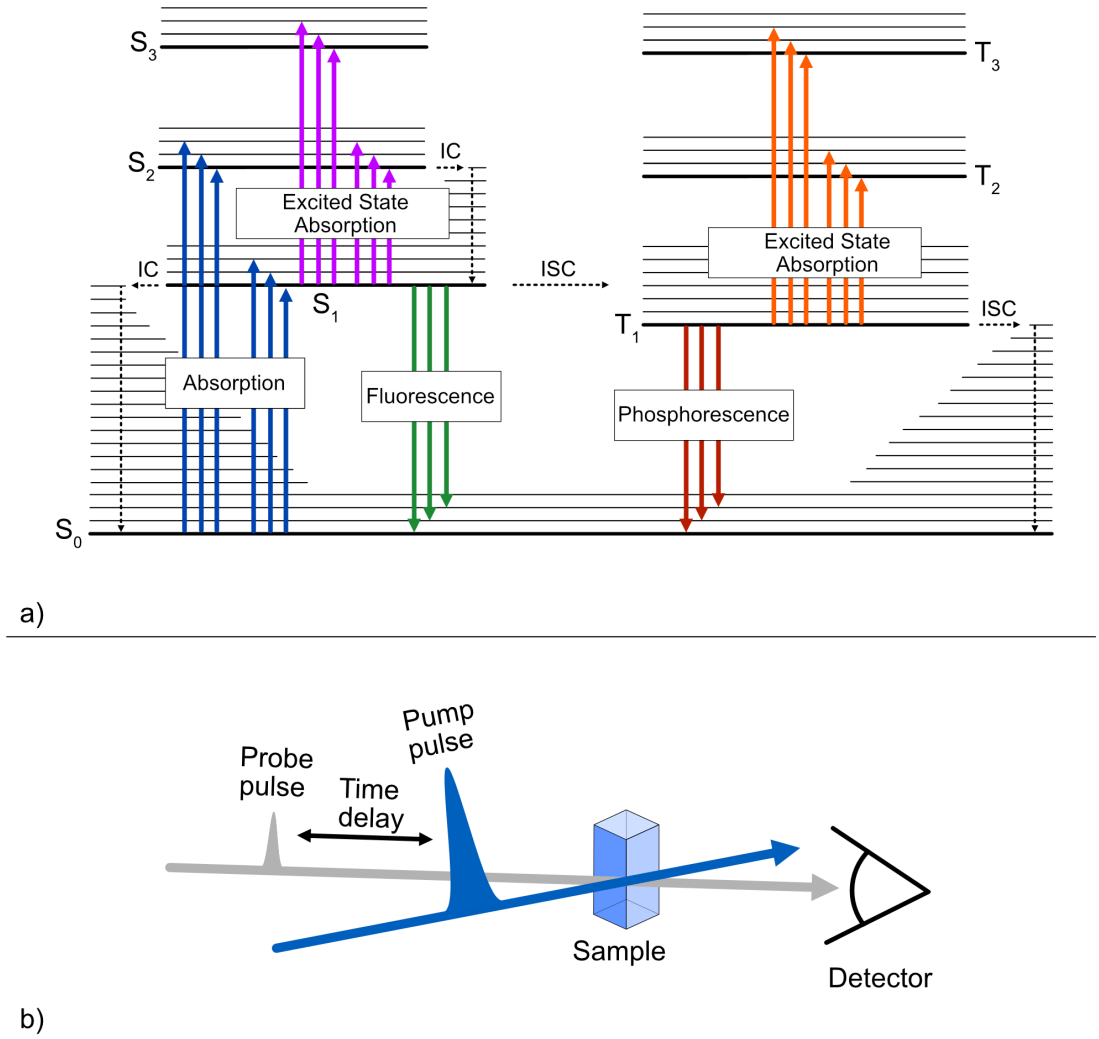

Figure 3.2: a) Modified Jablonski diagram which includes excited state absorption (ESA) for the singlet and triplet excited states. Photoexcitation and radiative decay are marked as solid lines and non-radiative processes are marked as dotted lines. b) Schematic illustration of TA showing how a sample is photoexcited by a pump pulse and then subsequently interrogated by a probe pulse after some time delay.

The time delay between the pulses can be varied. By scanning over a certain wavelength region while increasing the time between the arrival of the pump and the probe to the sample an absorption spectra, such as the one presented in Figure 3.3a, can be constructed.

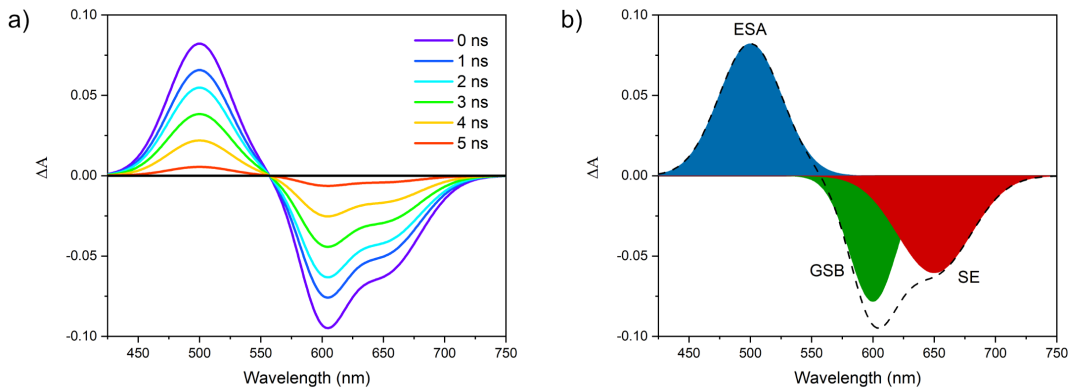

Figure 3.3: a) TA spectra showing the differential absorption as a function of wavelength and with different time delays between the pump and the probe in the legend. b) The corresponding TA spectra where the different contributions to the overall signal has been separated. ESA is an abbreviation for excited state absorption, GSB stands for ground state bleaching and SE means stimulated emission.

The data from a TA experiment is usually presented as a differential absorption spectra where the differential absorption (ΔA) is the absorption after the pump pulse (A_{I_+}) minus the absorption without the pump pulse (A_{I_-}) as shown in equation 3.3.

$$\Delta A = A_{I_+} - A_{I_-} = \log\frac{I_-}{I_+} \tag{3.3}$$

Here, ΔA is also expressed as the ratio between the probe light having passed through the sample with (I_+) and without (I_-) a preceding pump pulse, respectively. From this expression it can be seen that some parts of a TA spectra can have a net negative signal and some parts can be positive. There are in principle two main contributions that can give rise to negative signals. The first of these stem from the fact that when the pump beam interacts with the sample, a fraction of the molecules will leave the ground state and be transferred to the excited states. Consequently, the concentration of ground state molecules will decrease and the ground state absorption will decrease. As such, the absorption without a preceding pump pulse A_{I_-} can be larger than the value of the absorption shortly after the pump pulse A_{I_+} which will give a net negative ΔA. This is usually referred to as ground state bleaching (*GSB*) and is shown as the green area in Figure 3.3b. The second negative contribution is related to emis-

sion from the sample. More specifically it is related to stimulated emission (SE) (red area in Figure 3.3b) induced by the probe light with some minor contributions from spontaneous emission. This negative contribution can be understood by considering the transmitted intensities (I_+) and (I_-). Assuming that there is no absorption and only SE occurring at a particular wavelength, the number of photons received by the detector in absence of the pump (I_-) will be equal to the number of photons hitting the sample. Conversely, the signal with the pump active (I_+) will, again with the assumption of no absorption, result in the same amount of photons reaching the detector *plus* stimulated emission from the excited states that were populated by the pump. Since this will render $I_+ > I_-$, ΔA will become negative in accordance with equation 3.3. As a result, negative signals in a TA spectrum will resemble a combination of the steady state absorption and emission spectra. Finally, positive signals correspond to excited state absorption (ESA) which is shown as the blue region in Figure 3.3. This contribution will always be positive to the overall signal since it originates from absorption of excited states following the pump pulse. Note that the ESA can originate from not only singlet excited states, but from any transient species such as triplet states or charge-separated states that may evolve as a result of energy transfer or electron transfer from the initially excited specie. Careful analysis of the TA spectra can sometimes allow certain features to be assigned to a particular transition and the transitions are commonly denoted as S_1-S_n or T_1-T_n to indicate a transition from the first excited state to a higher excited state of singlet or triplet spin multiplicity.

3.2.1 Femtosecond and Nanosecond Transient Absorption

Both nanosecond (ns) and femtosecond (fs) TA have been used in this work. The time prefix indicates in what time domain the pulse width belongs to for each technique and this parameter also determines the time resolution of the measurement. Even though the two techniques are based on the same principle, the experimental setup and the information that can be acquired is quite different.
In nsTA the pulses typically have a width of a few nanoseconds and with this technique it is possible to monitor photoinduced processes in the order of a few tens of nanoseconds up to milliseconds. The probe lamp can on these timescales

be from a continuous light source and the delay between the pump and probe can be controlled electronically. In this thesis the pump pulse was generated by a Q-switched frequency tripled Nd:YAG laser with a fundamental output of 1064 nm and a pulse width of ∼7-10 ns. The desired excitation wavelength was obtained and tuned with an optical parametric oscillator (OPO). The probe light was detected with either a photomultiplier tube (PMT) for single wavelength dynamics or a charge coupled device (CCD) camera which produces a TA spectrum in a broader wavelength range.

With fsTA it is possible to monitor ultrafast processes that occur just a few hundreds of femtoseconds after the pump pulse. Contrary to nsTA it is not possible to electronically control the time delay between the pump and the probe pulse on these short timescales. Instead, the probe and pump pulse must originate from the same source and the delay between them is controlled by optical means. The setup used in this thesis consists of a mode locked Ti:Sapphire laser with an output of 800 nm, 80 MHz and a time width of approximately 200 fs. A regenerative amplifier pumped with a frequency doubled Nd:YLF laser is used to increase the power of the seed pulses. After the amplifier, the beam is split into a pump and a probe beam. The pump is directed through an optical parametric amplifier (OPA) which is used to obtain the desired excitation wavelength. The pump beam is subsequently guided towards an optical delay stage which can be adjusted to delay the arrival of the pump to the sample relative to the probe beam. The length of the optical delay stage thus determines the maximum time delay that can be probed and is for the setup used in this thesis 10 ns. After the delay stage the pump is focused and overlapped with the probe beam at the sample. The probe beam has at this point passed through a rotating CaF_2 plate which produces a white light continuum[49] and enables probing the transient absorption across a wide wavelength region with the help of a CCD camera.

3.3 Steady State Emission Spectroscopy

In steady state emission spectroscopy the sample is exposed to constant or pulsed illumination while the intensity of the emission is recorded by integrating over a certain time period. Figure 3.4 shows a schematic illustration of a typical emis-

sion spectrometer with a light source, a monochromator for the excitation light, a monochromator for the emission light and a detector that is placed perpendicular to the light source. An emission spectrum can be obtained by adjusting the emission monochromator and monitor the emission at different wavelengths while keeping the excitation light locked at a particular wavelength. It is also possible to monitor the emission wavelength while scanning over a range of excitation wavelengths. The spectrum acquired in this case is called an excitation spectrum and the excitation spectrum usually, but not always, closely resembles the absorption spectrum.[20]

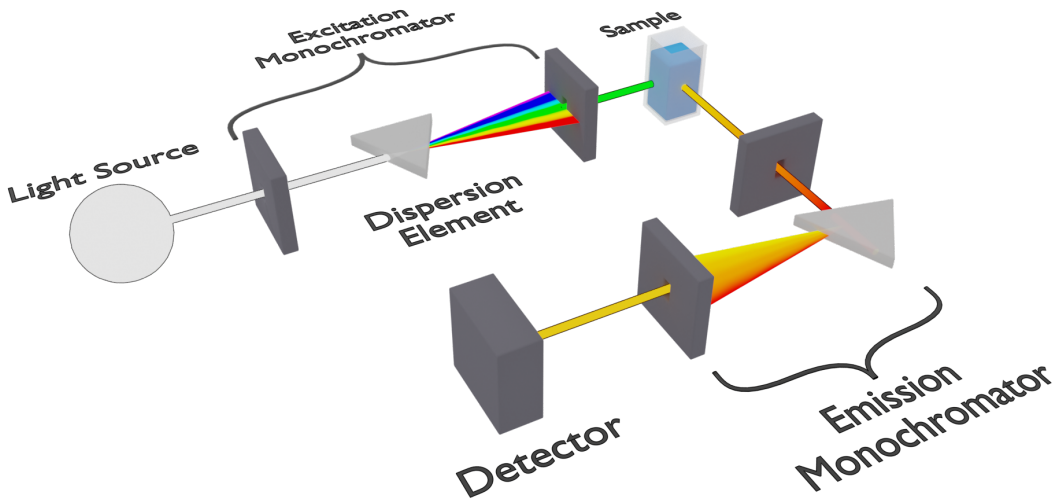

Figure 3.4: Schematic illustration of an emission spectrometer.

3.4 Time Resolved Emission Spectroscopy

Steady state emission spectroscopy is limited in the sense that it gives no information of how or when an excited state is deactivated. To remedy this issue, time resolved emission is utilized. The method which is used in this thesis to to measure emission lifetimes is called time correlated single photon counting (TCSPC). With this technique the sample is excited with a laser pulse that is typically much shorter than the emission lifetime under investigation. The overall time resolution of the measurement depends on the excitation pulse width in conjunction with the response time of the detector. The instrumental setup

used for the experiments presented herein utilizes a pulsed laser diode and a micro-channel plate photomultiplier tube (MCP-PMT) resulting in a combined time resolution down to 70 ps. The working principle of a TCSPC instrument is that the time between the excitation pulse and the arrival of the first photon at the detector is recorded. This process is repeated for a multitude of excitation pulses and eventually a histogram can be constructed with time on the x-axis and the number of photons on the y-axis. The measurement continues until enough photons have been accumulated for the measurement to be considered statistically significant (usually 5000 or 10000 photon counts in the top channel).[20] A schematic illustration of the instrumental setup is shown in Figure 3.5.

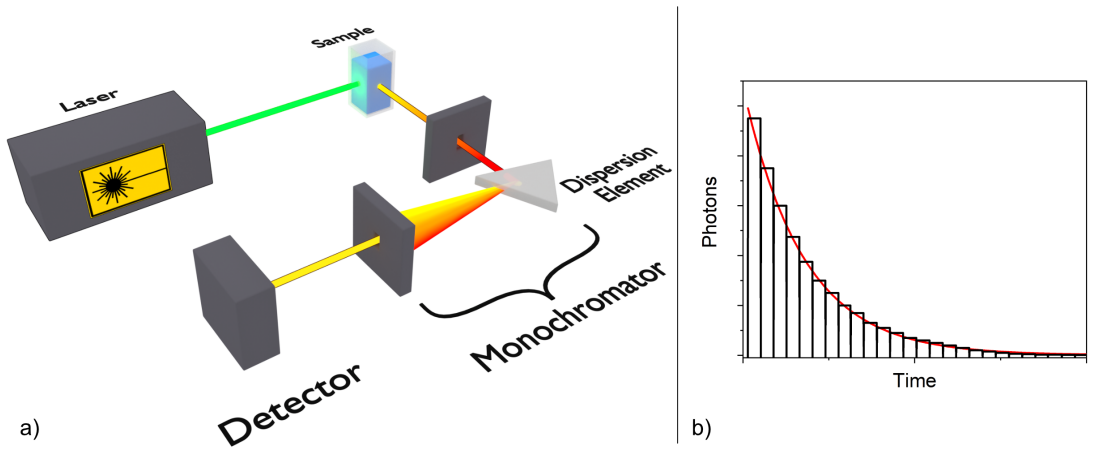

Figure 3.5: a) Schematic illustration of the experimental setup of a TCSPC instrument b) Example of a histogram from a TCSPC measurement where the red line represents an exponential fit to the data.

One of the most important parameters that can be obtained from a time resolved emission measurement is the lifetime (τ) of the emitting specie. The lifetime is defined as the average time the emitting specie remains in the excited state subsequent to being excited and it can be extracted from the histogram obtained from a TCSPC measurement. This can be realized by considering the rate expression for how an excited state decays with first order kinetics as shown in equation 3.4.

$$\frac{dN(t)}{dt} = -\frac{1}{\tau}N(t) \tag{3.4}$$

Here, *N(t)* is the excited state population which decays as a function of time (*t*)

and τ is the inverse sum of all first order rate constants that depopulate the excited state including both radiative and non-radiative processes. By integrating the expression and defining the initial population at *t=0* as N_0 one obtains the expression in equation 3.5.

$$N(t) = N_0\, e^{-(t/\tau)} \tag{3.5}$$

Finally, because the emission intensity *I(t)* is proportional to the excited state population *N(t)* it is possible to fit an exponential function directly to *I(t)* vs. *t* which is the output from a TCSPC experiment and where τ is the fitting parameter of interest that is extracted. The above description is however limited to a sample with a single emitting specie that only decays with a single, so called monoexponential lifetime. For systems containing more than one emissive specie or a single specie that has several lifetimes, the intensity vs. time plot can be fit to a sum of exponential decays according to equation 3.6.[20]

$$I(t) = \sum_i I_{0,i}\, e^{-(t/\tau_i)} \tag{3.6}$$

It should be noted that the validity of equation 3.6 is based on the assumption that the lifetime of the emission decay is much longer than the instrument response function (IRF) which in essence is the inherent time resolution of the instrument. If the lifetime of the emission is on the same time scale as the IRF it is necessary to deconvolute the exponential decay with the IRF since a significant fraction of the excited states formed by the early part of the pulse will start to decay at the same time as new excited states are populated from photons from the tail of the pulse. The convolution integral is presented in equation 3.7

$$I_{measured}(t) = \int_{-\infty}^{t} IRF(t')\, I(t-t')\, dt' \tag{3.7}$$

where $I_{measured}$*(t)* is the measured intensity decay and IRF(*t'*) is the intensity decay obtained when only scattered excitation light is allowed to reach the detector. When both $I_{measured}$*(t)* and IRF(*t'*) are known it is possible to solve for the true intensity decay *I(t)* which can be a sum of exponentials as in equation 3.6.[50]

3.5 Global Analysis of Spectroscopic Data

A time-resolved spectrum such as the one in Figure 3.3a) obtained from a transient absorption measurement is often not the result of absorption of a single species, but rather a linear combination of several individual absorption spectra from species that form and decay with different rates. For this reason it can be desirable to extract the spectral components that together forms the measured spectra and at the same time solve for the rate constants that governs the systems' dynamics by applying a kinetic model to the data. This can be accomplished using singular value decomposition (SVD) and global analysis. Here, global analysis refers to the simultaneous analysis of multiple decay traces at different wavelengths where the extracted fitting parameters (such as rate constants) can be shared for all the wavelengths or alternatively just be shared for a small part of the entire investigated spectral region.[51,52] SVD is a mathematical tool in linear algebra to factorize matrices. This tool serves two main purposes in the analysis of the raw data. The first is to extract the number of independent components that can describe the data set and thereby also reduce the amount of data that needs to be analyzed. The second purpose is to combine the extracted independent components with a kinetic model and calculate the true spectral components and their corresponding concentration time evolution.[53] The global SVD analysis starts with the experimentally obtained raw data in a matrix, A. The matrix A in the case of a transient absorption experiment consists of columns that correspond to absorption spectra at a certain time and rows that represent the time evolution of the absorbance at a specific wavelength. Thus, if the measurement had 400 wavelengths and 100 time steps, it would be a 100×400 matrix. The process of SVD separates the matrix A into a product of three matrices U, S and V according to equation 3.8.

$$A = USV^T \tag{3.8}$$

Here, the matrix U contain the column space of A which corresponds to information about the spectrum at different times. The matrix V contain the row space of A which represents the time evolution of the absorption at individual wavelengths. The third matrix, S, is a diagonal matrix and the values of the diagonal elements in S are weights (or so called singular values) that determines the

importance, or equivalently, the relative amount of information in the columns in U and V. Each column of U and V will carry less relevant information in a progressive manner and this is reflected in the diagonal scalar values of S which also decreases until a plateau value of zero. The plateau value indicates that the columns after this point in U and V are superfluous and only carry noise. This is the first part of the SVD analysis which, as previously stated, has the main purpose of finding the number of independent components that can accurately describe the absorption spectra of the raw data in A. The next step is to reduce the matrices U, S and V and only keep the columns that are significant. The matrices are reduced based on analysis of the diagonal values in S and typically the significant columns are the ones before the previously described plateau value. This should also coincide with the columns in U and V, respectively, that do not show clear spectral features. All columns beyond the last significant column are discarded and the result is a reduced matrix A_r as seen in equation 3.9.

$$A_r = U_r S_r V_r^T \tag{3.9}$$

It is important to note that at this point the independent orthogonal components from the reduced matrices U_r and V_r have no real physical meaning since there are a multitude of solutions to equation 3.8. This is where the second part of the SVD analysis enters the picture. The first step of this second part is to define a kinetic model describing how the different absorbing species are related to each other. This step is of paramount importance since there may be several models that can be fit to the experimental data. The model should be chosen while taking into account the number of significant components from the prior SVD analysis as well as any additional knowledge about the system the experimenter might have. An example of such a kinetic model is provided in Figure 3.6 where the concentration matrix (C) is found as the solution to the differential equation system involving the relevant combination of rate constants according to first order kinetics (which most photophysical processes are assumed to follow).

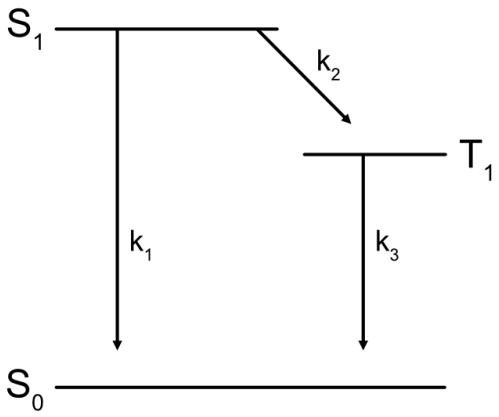

$$\frac{dC}{dt} = KC$$

$$\Updownarrow$$

$$\frac{d}{dt}\begin{pmatrix} c_{S1} \\ c_{T1} \end{pmatrix} = \begin{pmatrix} -k_1-k_2 & 0 \\ k_2 & -k_3 \end{pmatrix}\begin{pmatrix} c_{S1} \\ c_{T1} \end{pmatrix}$$

Figure 3.6: Left: Jablonski diagram of a hypothetical kinetic situation involving decay from a singlet excited state (S_1) to the ground state (S_0) or first triplet excited state (T_1). Right: Differential equation system for the kinetic scheme to the left.

The time dependent concentration matrix C is connected to V_r and is ultimately found by matrix rotation of V_r with the rotation matrix (R) according to equation 3.10.

$$V_r = RC \tag{3.10}$$

Similarly, the true spectral components are found in equation 3.11 by matrix rotation of U_r with the same rotation matrix resulting in a new matrix, B, which contains the true absorption spectra of each component according to the chosen model.

$$U_r = RB \tag{3.11}$$

The fitting process is repeated many times while minimizing the least square difference between the raw data matrix A and the simulated spectra which corresponds to the product of B and C: ($|A\text{-}BC|$).[53–55] The obtained spectral components are commonly referred to as evolution associated spectra (EAS) in the case of a consecutive model where one specie converts to another specie in a sequential manner (for instance: A→B→C→ground state). The spectral components can also be referred to as species associated spectra (SAS) if a specific model is applied which includes both parallel and sequential decays.[51]

SVD can be very helpful and valuable in the analysis of spectroscopic data. There are, however, several pitfalls that one should be aware of when analysing data using this method. One of the most important factors to consider is the impact of the initial start guesses for the fitted parameters. Start guesses are required to start the fitting process, but great care must be taken to make sure that the initial guesses are good enough. The reason for this is that the fitting algorithm tries to find a minimum in a multidimensional surface of the sum of the residuals vs. every parameter that can influence it (residuals refers to the difference between a measured and a fitted value). This multidimensional surface contains both local and global minima and if the start guess is chosen poorly there is a risk that the starting point of the iteration is on the inner side of one of the local minima. This will result in that the solution converges to the local minima and ultimately the wrong answer is obtained from the fitting procedure. One way to circumvent this problem is to try with a multitude of starting guesses and observe the robustness of the fit. Another commonly employed strategy is to initially lock certain parameters (the ones that the experimenter is most sure about) and let the remaining parameters be fit with this constraint. Once a fit has been achieved in this way one can release one parameter at a time and approach a solution that best fit the data. This is particularly useful in fits which involve many parameters. Care must also be taken to avoid overparameterization, which occurs when more parameters than necessary are used to fit the data. This often results in low robustness, i.e. that different solutions are obtained for different starting guesses while still having a more or less equal sum of square errors. In addition to checking for robustness, it is also possible to avoid overparameterization by analysing the dependency of each parameter with the others. Furthermore, overparameterization usually results in large standard error values. In conclusion, SVD is a powerful tool for analysis and deconvolution of complicated spectroscopic data, but it comes with certain limitations that must be considered. One of the the most important countermeasures against faulty fitting is the knowledge of the experimenter themselves and their ability to recognize some solutions as unrealistic or improbable.[53,55]

4

Results and Discussion

This chapter presents two separate investigations on SF. The first is concerned with how the conformational geometry of two covalently bound pentacene molecules affects the rate of intramolecular SF and the lifetime of the formed triplet-pair. The second part of this chapter is focused on **DPIBF** monomers bound to different mesoporous semiconductors. Here, intermolecular SF of **DPIBF** and the possibility of PET subsequent to the SF event is investigated by chemisorption of **DPIBF** to TiO_2, ZrO_2 and SnO_2 films in solvents of varying polarities.

4.1 Molecular Rotational Conformation and Singlet Fission

This section summarizes the main findings from **Paper I**[56] in which SF and its dependence on rotational conformation and molecular orientation was carefully studied. For this purpose, three pentacene dimers were synthesized and their molecular structures are presented in Figure 4.1 together with the structure of the pentacene monomer 6,13-Bis(triisopropylsilylethynyl)pentacene (**PM**), which is a well-known SF molecule. In all three dimers the pentacene moieties are connected by a 1,4-diethynylphenylene spacer with the intention of allowing rotation of the pentacene units relative to one another. Two of the dimers were further modified with substituents on the central phenylene unit. The large and bulky nature of the substitients introduces steric hindrance that restricts the rotational freedom and additionally has the potential to shift the equillibrium distribution of the conformational geometries. Figure 4.1b) shows the steady state absorption spectra of PM and the three dimers in room temperature. Although there are clear general similarities between the dimer and monomer spectra there are some distinct differences indicating substantial electronic interaction between the pentacene moieties.

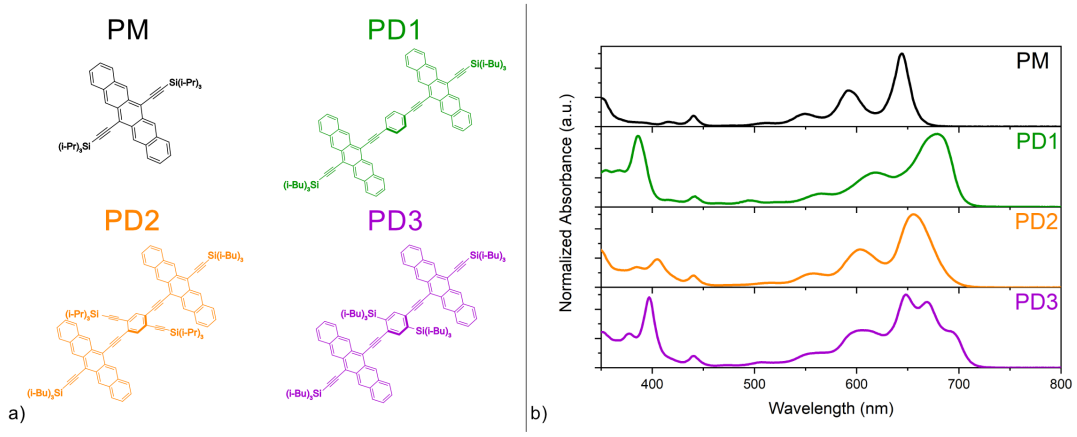

Figure 4.1: a) Molecular structures of 6,13-bis(triisopropylsilylethynyl)pentacene (**PM**) and the dimers **PD1**, **PD2** and **PD3** investigated in this study. b) Steady state absorption spectra of PM and the dimers.

Furthermore, the absorption bands of the dimers are broadened relative to the spectra of the monomer. This can be interpreted as that each dimer can adopt a multitude of different conformations owing to the rotational freedom around the ethynyl groups in the spacer. Thus, at room temperature there will be a distribution of conformations each with absorption transitions at slightly different energies. To lend credence to this statement density functional theory (DFT) calculations were performed to investigate the rotational freedom of each of the dimers around the central diethynylphenylene spacer. This was done by first calculating the lowest energy conformations that the dimers can adopt. The optimal structure will be a function of the amount of conjugation across the entire molecule, which will lower the potential energy, and repulsive forces from the steric hinderence caused by the bulky side groups on the central phenylene unit which will raise the potential energy of the system. The obtained optimum structures are presented in Figure 4.2a).

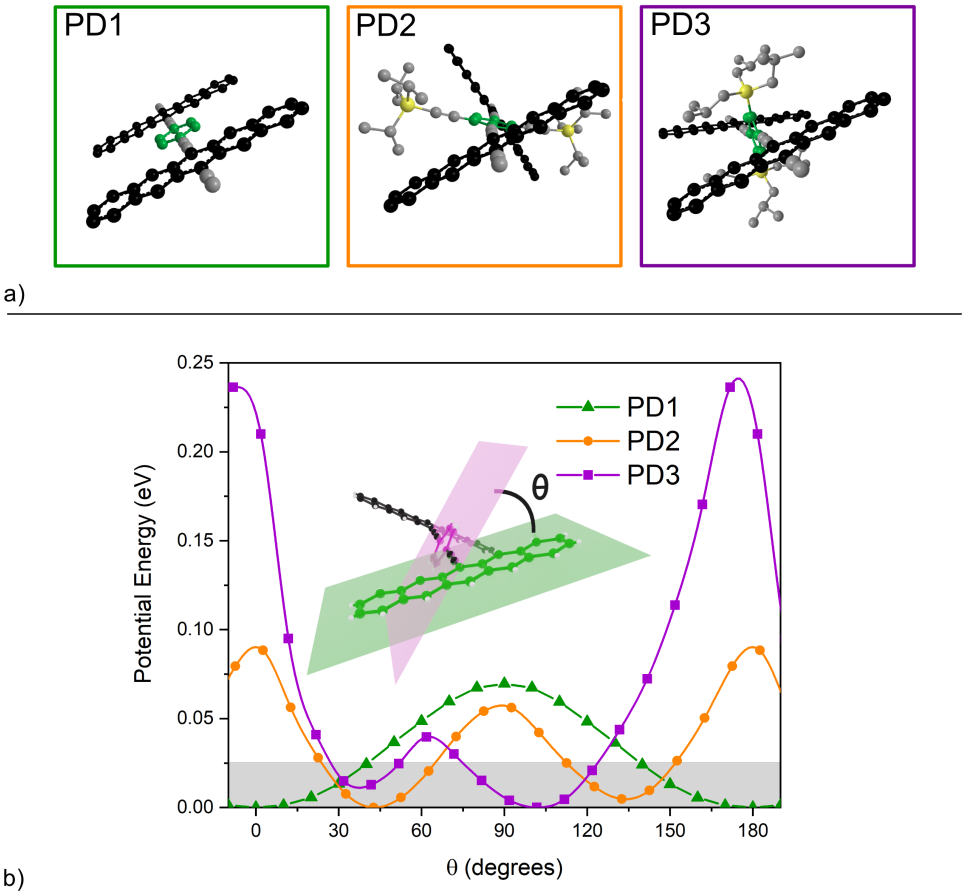

Figure 4.2: a) Lowest energy conformations of **PD1**, **PD2** and **PD3**. b) Potential energy landscape obtained by scanning over a range of dihedral angles θ. Thermal energy at 295 K is highlighted by the shaded area.

The unsubstituted dimer **PD1** adopts a totally coplanar structure in its lowest energy conformation. **PD2** and **PD3** on the other hand have conformations that are more twisted due to steric hinderence. These conformations are however merely the conformations that the molecules will adopt at 0 K. At room temperature there will, as previously stated, exist a distribution conformations. In order to map the potential energy V(θ) of different conformations relative to the lowest energy conformation a relaxed scan of the dihedral angle θ was performed. Here, θ is defined as the angle formed between the plane of one of the pentacene units and the plane formed by the central phenylene unit as shown in the inset of Figure 4.2b). A relaxed scan means that θ was set to a certain value and then all other coordinates were allowed to relax to find the lowest energy conformation of that particular θ. The result of the relaxed scan is shown in Fig-

ure 4.2b) where thermal energy at 295 K is included as the shaded area. From this it is clear that there are a large number of conformations close in energy to the lowest energy conformations and that most of them will be present together in a sample at room temperature. It can also be deduced from the scan that the rotational barrier is largest for **PD3**, then **PD2** and finally lowest for **PD1**, which will be important to consider for the fsTA measurements of the dimers as shown in Figure 4.3.

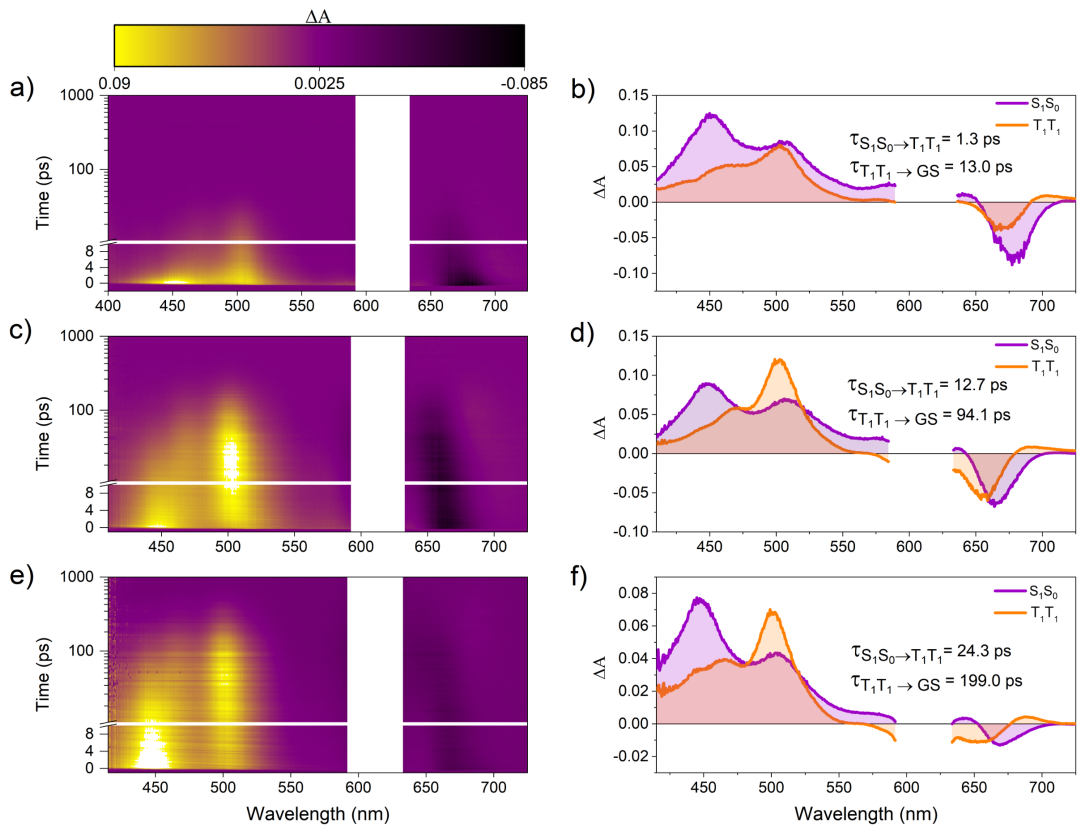

Figure 4.3: Room temperature fsTA spectra and corresponding evolution associated spectra (EAS) of dimers (a and b) **PD1**, (c and d) **PD2**, and (e and f) **PD3**. The kinetics of all three dimers could be accurately described by a two-component sequential model $S_0S_1 \rightarrow T_1T_1 \rightarrow$ ground state (GS) using global analysis with components and lifetimes indicated in the figure. The measurements were performed in toluene with a pump pulse at 612 nm and the pump scatter near the excitation wavelength has been removed for clarity.

fsTA was used to experimentally determine the influence of the central phenylene unit substitutions on the SF dynamics. The room temperature fsTA spectra and their corresponding evolution associated spectra (EAS) of all the dimers are

presented in Figure 4.3. All of the dimers can be accurately modeled with a consecutive model of two components where the first converts to the second. The two components have a unique spectroscopic signature but are more or less identical across the dimer series. The first component is in all cases formed immediately following excitation and display absorption maxima at 460 and 510 nm. This is assigned to absorption of the singlet excited state S_1S_0 since it is formed instantaneously and also matches the initial spectra of the monomer **PM** in solution. The singlet excited state has a very short lifetime and evolves into the second component within 1 to 25 ps for every dimer. The second component is assigned to be the correlated triplet pair (T_1T_1) based on its similarity with the sensitized triplet spectra as seen in Figure 4.4 where the sensitized triplet spectra of **PD2** is compared to the second component from the fsTA spectra in Figure 4.3. **PD2** is just shown as an example here and the T_1T_1 component of **PD1** och **PD3** also match their corresponding sensitized triplet spectra as can be seen in **Paper I**.

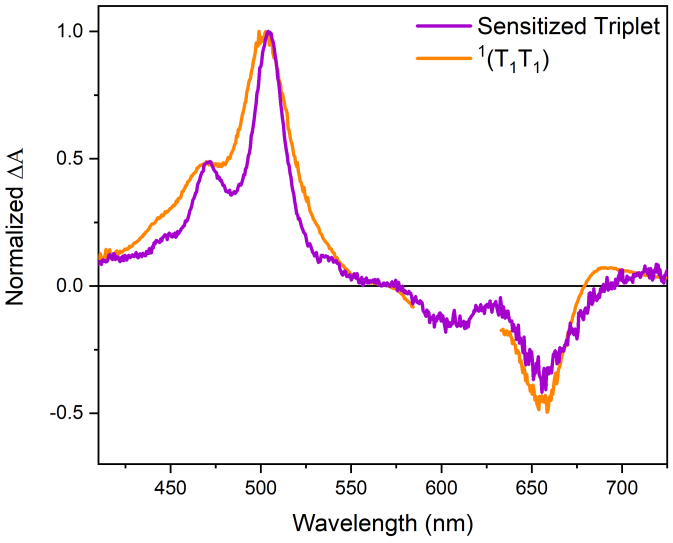

Figure 4.4: Sensitized triplet excited state spectra (purple) of **PD2** obtained via triplet energy transfer from platinum octaethylporphyrin (**PtOEP**) in toluene solution together with the triplet pair EAS of **PD2** (orange) obtained from the SVD analysis as shown in Figure 4.3. A similar comparison of sensitized triplet spectra and triplet pair EAS of **PD1** and **PD3** is presented in **Paper I**.

The ultra-fast formation of the triplet pair is solid evidence that the triplet for-

mation observed is a result of SF and not ISC since ISC typically occurs on much longer time scales for organic molecules. Furthermore, the relatively short lifetime of sub 200 ps in the longest case for **PD3** indicates that no fully independent triplet states are formed and that the correlated triplet-pair is deactivated to the ground state before the triplets can dissociate. Notably, the rate of formation and decay of the triplet pair is largest for **PD1** followed by **PD2** and finally **PD3** and as such it follows the trend of rotational freedom since **PD1** is the least rotationally restricted dimer followed by **PD2** and then **PD3**. Based on the presented results it appears as if the fsTA spectra presented here are the average SF kinetics of a distribution of different conformers where some do SF very fast and efficiently and some a little bit slower. However, on average, the more restricted and twisted the dimers **PD2** and to an even larger extent **PD3** display the least efficient SF.

To further support the hypothesis that the different conformers present in the sample have absorption transitions at different energies time dependent DFT (TD-DFT) calculations were employed. The result of these calculations are presented in the top part of Figure 4.5. The vertical colored bars represent the lowest energy transitions corresponding to a conformation of a specific orientation of the pentacene units relative to the central phenylene unit as indicated in the inset. The bottom part of Figure 4.5 show the steady state absorption of **PD1** and **PM** showing that the theory in general matches well with the experimental results. It should be noted that the calculation do not take vibrations into account and thus lack the vibronic progression that is observed in the experimental data. The calculations here shows that the more coplanar geometry of the conformer the more red-shifted is the absorption transition. This is reasonable since this conformation is expected to be the most conjugated and have the strongest electronic coupling. These results can also explain the blue shift of the GSB in the fsTA spectra in Figure 4.3 at $\sim$650 nm for later time delays between the pump and the probe. This blue shift likely corresponds to that the more red-shifted and more strongly coupled conformations undergo SF fast and efficiently while less strongly coupled conformers that have ground state absorption at shorter wavelengths remain in the singlet excited state even at longer time delays.

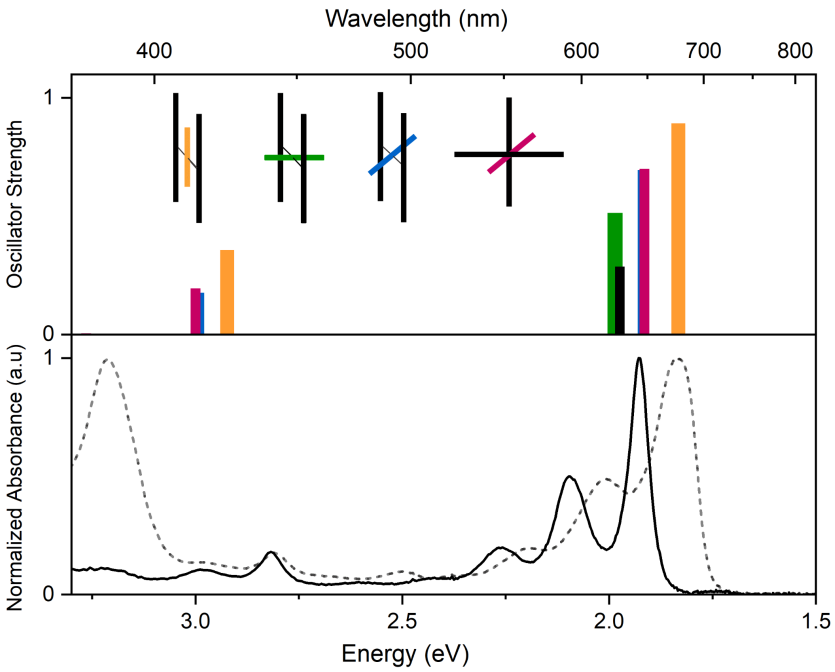

Figure 4.5: Top: Lowest energy transitions in different conformations of an unsubstituted pentacene dimer (**PD1**, orange, red, blue and green bars) and the monomer (**PM**, black bar), calculated using TD-DFT. The inset illustrates the pentacene-phenylene-pentacene geometry of the respective conformer. The shorter colored bars represent the phenylene-bridge unit at different dihedral angles and the longer grey bars represent the pentacene moieties. Note that the blue and red conformations with $\theta = 45°$ have very similar transition energies and oscillator strengths causing their bars to overlap. Bottom: Steady state absorption spectra of **PD1** (dashed) and **PM** (solid) in toluene.

4.1.1 Selective excitation of rotational conformers

Based on the above results we speculated that it could be possible to selectively photoexcite different conformers and observe different SF rates for the same dimer molecule by simply using different excitation wavelengths. However, as previously mentioned and demonstrated, at room temperature the different conformations have overlapping absorption bands leading to excitation of a range of conformers at any given excitation wavelength. A solution to this could be to lower the temperature since this could provide a more narrow distribution. An estimation of the distribution of conformers at different temperatures can be obtained by using the relative potential energy V(θ) of the various conformers in Figure 4.2 in the Boltzmann distribution function presented in equation 4.1.

$$P(\theta, T) = \frac{e^{-V(\theta)/k_B T}}{\int e^{-V(\theta)/k_B T} d\theta} \tag{4.1}$$

The resulting probability distribution as a function of the dihedral angle θ and temperature is shown in Figure 4.6.

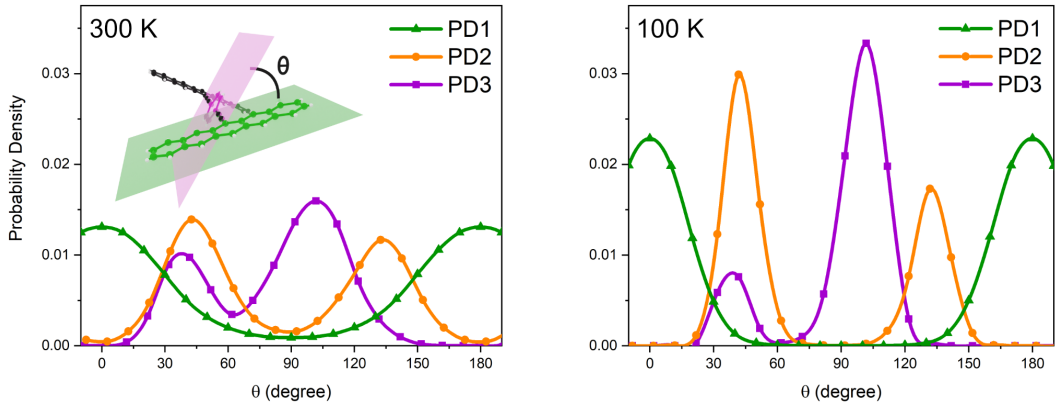

Figure 4.6: Probability distribution function of the dimers' rotational conformers at 300 K and 100 K.

At room temperature, a large range of conformers are available to **PD1**, **PD2**, and **PD3**. However, the probability distribution is significantly narrower at 100 K and at this low temperature a larger fraction of the dimers belong the the conformers of lower energy. Indeed, the steady state absorption of **PD3** in Figure 4.7a) shows that the absorption bands become narrower and more clearly resolved at 100 K compared to room temperature. **PD3** is shown as an example here but similar changes are observed for all dimers upon cooling. Notably, the red-edge of the lowest energy absorption band grows significantly. This is an indication that a large fraction of the dimers in the sample adopt a more strongly coupled conformation with red-shifted absorption at lower temperatures. This conclusion is supported by both the blue shift of the GSB at longer time delays in the fsTA room temperature measurements in Figure 4.3 and the theoretical calculations in Figure 4.5 where it was shown that more co planar conformations have absorption at lower energy. Based on these findings, fsTA measurements at 100 K in 2-methyltetrahydrofuran (MTHF) were performed on all of the dimers. Figure 4.7b) show the single wavelengths dynamics of the triplet pair of PD3 when excited with different excitation wavelengths.

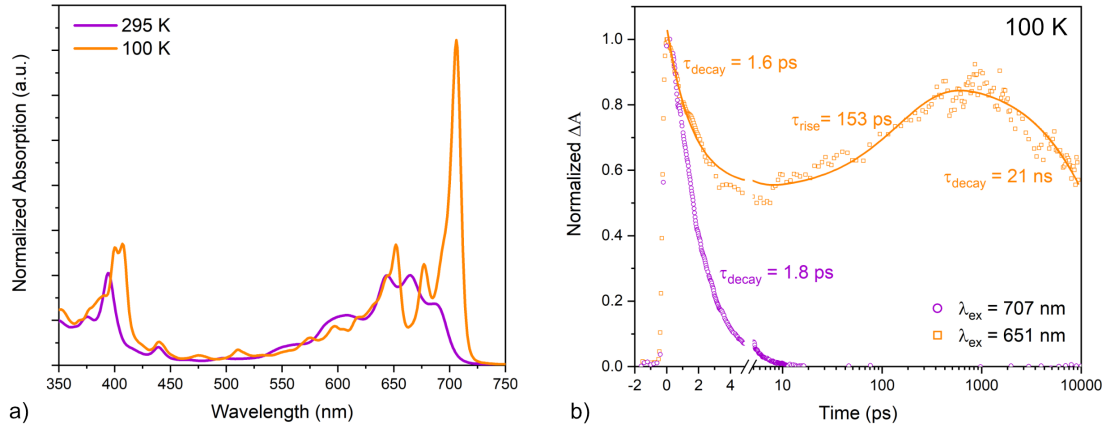

Figure 4.7: a) Steady state absorption spectra of **PD3** at 295 K and 100 K. b) fsTA single wavelength kinetics of the triplet-pair peak of **PD3** at 505 nm for with an excitation wavelength of 707 nm and 651 nm at 100 K in MTHF.

Exciting at the red edge of the steady state absorption at 707 nm the formation of the triplet pair occurs within the instrument response time of the system (∼250 fs). With this excitation wavelength the triplet pair also decays very rapidly with a lifetime of roughly 1.8 ps. In contrast, when shifting the excitation wavelength to 651 nm the kinetics are more complicated and involves species with several different lifetimes. There is a slower rise of the signal at later times where a species form in 153 ps and decay in 21 ns suggesting that excitation at 651 nm results in the population of a more weakly coupled conformer that performs slower SF. Furthermore, it appears as if this excitation wavelength also excites a very strongly coupled conformer that displays kinetics similar to the one that was observed with excitation at 707 nm. The reason for this is likely due to the fact that the conformer with its first absorption transition at 707 nm has a vibronic progression that extends to shorter wavelengths and overlaps partly with conformers of weaker coupling at higher energy.

4.1.2 The effect of viscosity on excited state dynamics

The fsTA measurements at 100 K in MTHF reveals that the conformers that are not strongly coupled have much longer triplet pair lifetimes compared to the lifetimes observed at room temperature. At 100 K, MTHF is close to the glass transition temperature and will be highly viscous or even more or less solid.[57]

In this environment the movement of the dissolved molecules will be limited and the rotation of the pentacene moieties relative to one another in the dimers will be very slow. It is possible that the limited rotational freedom in this environment is the underlying reason for the longer triplet lifetimes. To gain more insight into the excited state dynamics and its dependence on viscosity, fsTA was performed on the dimers dissolved in highly viscous polystyrene films. The single wavelength fsTA kinetics of the triplet pair at 505 nm for **PD3** is presented in Figure 4.8 where the rate of formation and decay of the triplet pair in toluene and in polystyrene are compared. Interestingly, the rate of formation of the triplet pair, i.e. the SF rate, is similar in the high and low viscosity environment as can be seen by comparing the rise times of the signal which is 28 ps for toluene and 46 ps for polystyrene. However, the lifetime of the triplet pair is almost 45 times longer in polystyrene. Keeping in mind that these measurements were performed at room temperature and thus gives the average kinetics of many conformers this result indicates that the SF event that initially produces the correlated triplet pair is not strongly dependent on conformational changes in the excited state. In contrast, it seems that the decay of the triplet pair to a larger degree requires a conformational change to a more strongly coupled geometry.

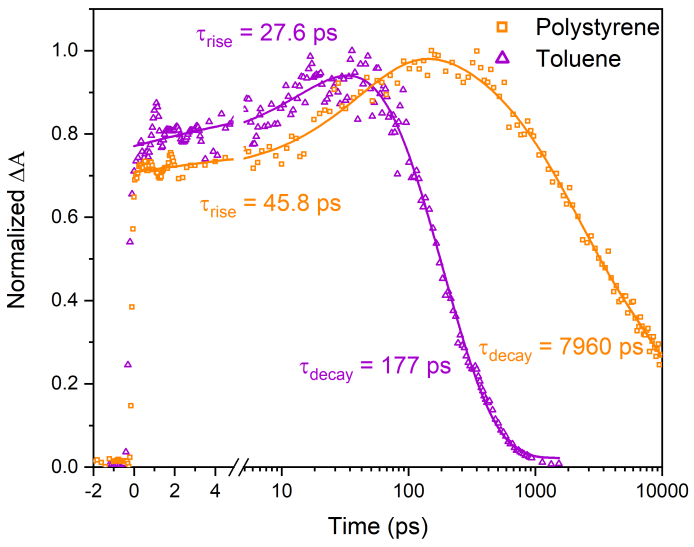

Figure 4.8: Room temperature fsTA single wavelength kinetics of the triplet-pair peak of **PD3** at 505 nm in toluene and in polystyrene obtained with a pump pulse at 612 nm.

4.1.3 Summary

In summary, the conformational dependence of SF in pentacene dimers has been experimentally investigated and theoretical calculations have been used to support the conclusions. Selective photoexcitation of different conformers have revealed that a dimer can have several orders of magnitude different SF rate and triplet pair recombination rate depending the conformation that is initially photoexcited. Furthermore, studies in environments of varying viscosity have shown that triplet pair recombination is heavily dependent on conformational relaxation in the excited state whereas the rate of triplet formation is largely unaffected by increasing the viscosity. Since it is rare to have efficient SF together with slow triplet recombination in a single system this design parameter could be important for future applications which will likely require both quantitative SF and triplet states that are long lived.

4.2 Singlet Fission and Electron Injection into Mesoporous Semiconductors

This section presents the central results from **Paper II**[58] where the SF and electron injection capabilities of a derivative of diphenylisobenzofuran (**DPIBF**) when attached to various thin film mesoporous semiconductors was investigated. The mesoporous semiconductors used in this work (SnO_2, TiO_2 and ZrO_2) were fabricated by applying a colloidal solution consisting of nanoparticles with a diamater of 5-25 nm to a glass slide. Swiping a glass rod across the solution on the glass slide while using a piece of scotch tape as spacer produces thin films that after sintering has a thickness of roughly 2-6 μm. The resulting mesoporous structure has a large surface area that is well-suited for the purpose of attaching many molecules with short intermolecular distances. The attachment of **DPIBF** to the semiconductor surfaces was achieved by modifying **DPIBF** with a carboxylic acid functional group and the mechanism involves a covalent bond formation between the oxygens of the carboxylic acid to the metal atom in the semiconductor.[59] The molecular structures of **DPIBF** and the functionalized derivative (**DPIBF-C6**) are presented in Figure 4.9a). As evident from Figure 4.9a) the carboxylic acid is separated from the **DPIBF** moiety with a hydrocarbon chain consisting of six carbons, hence the name **DPIBF-C6**. The alkane spacer serves two main purposes. Firstly, the spacer should in theory provide some freedom for the **DPIBF** moieties to move and orient themselves to favourable positions relative to neighbouring **DPIBF-C6** molecules to ensure efficient SF. Secondly, the alkane chain introduces a short distance between the semiconductor surface and **DPIBF**. The added distance could potentially reduce the probability of electron injection from the singlet excited state of **DPIBF-C6** before SF has any chance to occur. This is important to consider since the overall aim of the project is to first have SF occur and then subsequently have electron injection from each of the formed triplet excited states. Of course, the increased distance will not only reduce the electron injection rate from the singlet excited state, but also from the triplet excited state. However, since triplet excited states generally have orders of magnitude longer excited state lifetimes than singlet excited states the electron injection from the triplets should be less affected by the increased distance

since they will, on average, have more time perform the electron injection than the singlets.

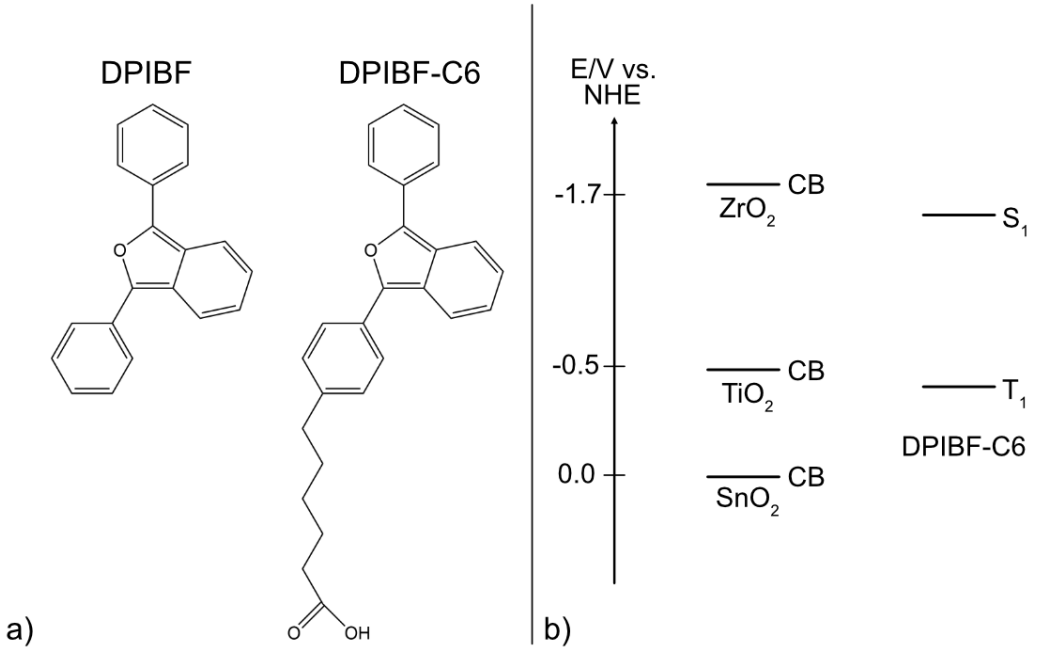

Figure 4.9: a) Molecular structures of 1,3-diphenylisobenzofuran **DPIBF** and its carboxylic acid modified derivative **DPIBF-C6**. b) Relative energies of the singlet and triplet excited state reduction potentials of **DPIBF-C6** together with the CB edge energy of ZrO_2, TiO_2 and SnO_2.

The semiconductors used here were selected because of their distinctly different band gaps and CB edge energies which allowed us to investigate the photophysical processes of **DPIBF-C6** on the surface with varying driving force for the electron injection. The electron injection driving force from **DPIBF-C6** to the different semiconductors can be estimated by comparing the excited state oxidation potential of the donor (**DPIBF-C6**) with the conduction band levels of each of the semiconductors, respectively. This is in essence a slightly simplified version of equation 2.9. The oxidation potential of the first singlet excited state S_1 and the first triplet excited state T_1 of **DPIBF-C6** can be obtained by taking the value of the ground state oxidation potential and subtracting the excitation energy of the respective excited states. The conduction band edge energies and the oxidation potentials of **DPIBF-C6** are presented in Figure 4.9b).[35,60–66] The conduction band edge of ZrO_2 is higher in energy than both the oxidation potential of **DPIBF-C6** S_1 and T_1. Consequently, there should be more or less no

driving force for electron injection from either the singlet or triplet excited state to ZrO_2, which will serve as a reference where the photophysics of **DPIBF-C6** can be studied in absence of electron injection. For TiO_2 the conduction band edge is significantly lower in energy compared to **DPIBF-C6** S_1 which should provide substantial driving force for the electron injection. The triplet excited state oxidation potential on the other hand is marginally lower in energy than the conduction band of TiO_2 and electron injection will thus not likely be very effective. However, electron injection from **DPIBF-C6** T_1 should in this case still be considered even though the process appears to be slightly uphill in energy. The reason for this includes the possibility of some experimental errors in the determination of the presented values and additionally some general uncertainty in semiconductor energy levels since they can be slightly altered as a result of chemisorption of molecules.[67,68] Finally, the conduction band of SnO_2 is well below the oxidation potential of both the S_1 and T_1 oxidation potentials rendering electron injection from both states energetically possible. A schematic illustration of the combined system of mesoporos semiconductor network with the attached **DPIBF-C6** is presented in Figure 4.10. It should be mentioned that ZrO_2 and the other semiconductors TiO_2 and SnO_2 have wide bandgaps and are not directly optically excited by the excitation wavelengths used herein.

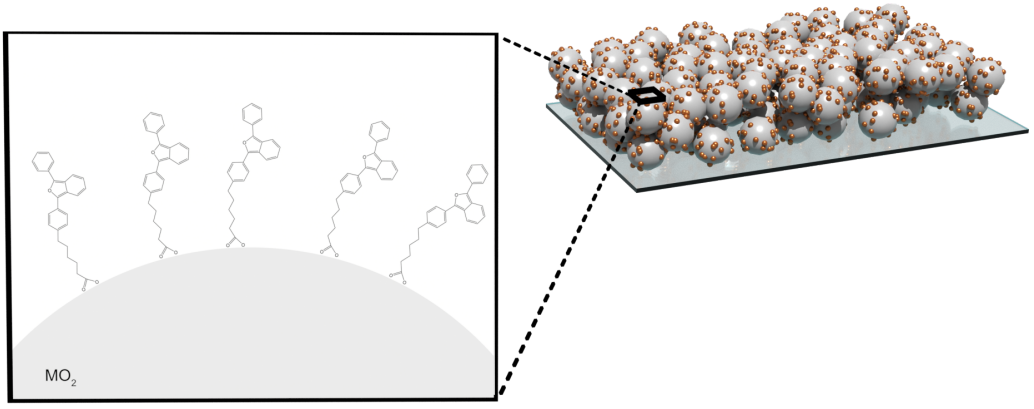

Figure 4.10: Schematic illustration of a thin film consisting of a mesoporous network of either SnO_2, TiO_2 or ZrO_2 on a glass substrate with **DPIBF-C6** chemisorbed to the surface of the semiconductor nanoparticles.

In the following sections the characterization of **DPIBF-C6** in different environments will be presented starting with a comparison of the fluorescence efficiency in solution and when attached to semiconductor surfaces.

4.2.1 Fluorescence properties of DPIBF-C6 in different environments

When **DPIBF-C6** is dissolved in solution and not attached to a semiconductor surface the compound has a fluorescence quantum yield close to unity and a lifetime of around 5 ns with an emission maximum at ~460 nm. In contrast, when **DPIBF-C6** is bound to any of the semiconductors used in this study the emission is heavily quenched indicating that additional processes occur on the surface and that they occur faster or on the same time-scale as the fluorescence. The time resolved emission of **DPIBF-C6** in solution and when attached to ZrO_2 is shown in Figure 4.11.

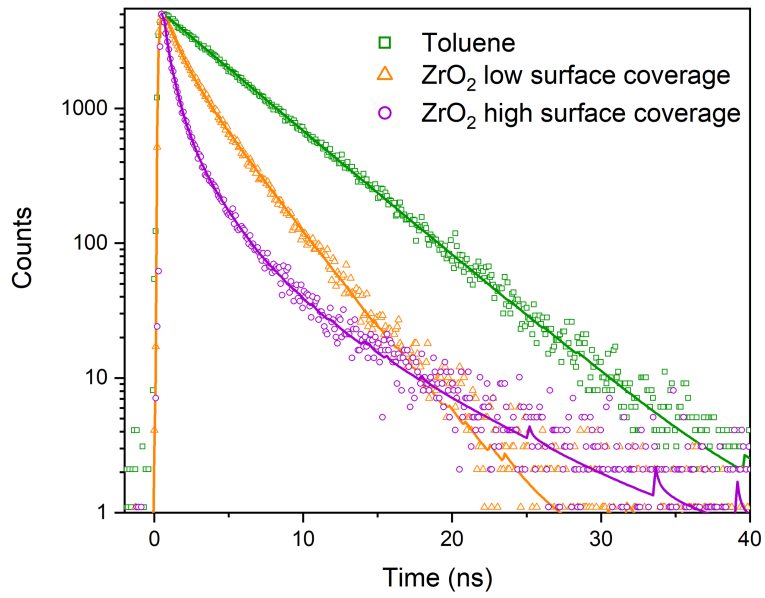

Figure 4.11: Time resolved emission of **DPIBF-C6** in toluene and when attached to ZrO_2 immersed in toluene with high and low surface coverage. The emission was monitored at 500 nm and the sample was excited at 405 nm.

Contrary to the monoexponential lifetime in solution the quenched emission of **DPIBF-C6** on ZrO_2 requires several lifetimes to be accurately modeled. Importantly, the average lifetime is progressively more quenched as the concentration on the surface is increased indicating that SF or some other process requiring

close contact between molecules is responsible for the quenched emission. Interestingly, the emission decay of **DPIBF-C6** on TiO_2 (not shown here) does not display a clear concentration dependence. A possible explanation for this could be that electron injection from the singlet excited state is the dominating process for all surface coverages on this substrate. The concentration dependence is however seen again for SnO_2 (shown in **Paper II**) which suggests that SF might occur to a larger degree in this case. To get more information regarding exactly which process is favoured in each case we turn to fs- and nsTA.

4.2.2 Photophysics of DPIBF-C6 in solution and triplet sensitization

The TA spectra of **DPIBF-C6** attached to the surface of the semiconductors will consist of overlapping ESA transitions from different species such absorption from the singlet excited state, triplet excited state and potentially charge separated states. To get a better idea of their individual spectroscopic signatures the singlet and triplet ESA spectra were investigated separately. Since the quantum yield of fluorescence in solution is close to unity it can be concluded that the efficiency of ISC is very low. Consequently, the fsTA spectra of **DPIBF-C6** in dilute solution should almost exclusively consist of ESA bands from S_1-S_n transitions together with negative contributions from stimulated emission and GSB. The steady state absorption and emission spectra of **DPIBF-C6** and the fsTA spectra of **DPIBF-C6** in toluene are presented in Figure 4.12a) and b), respectively.

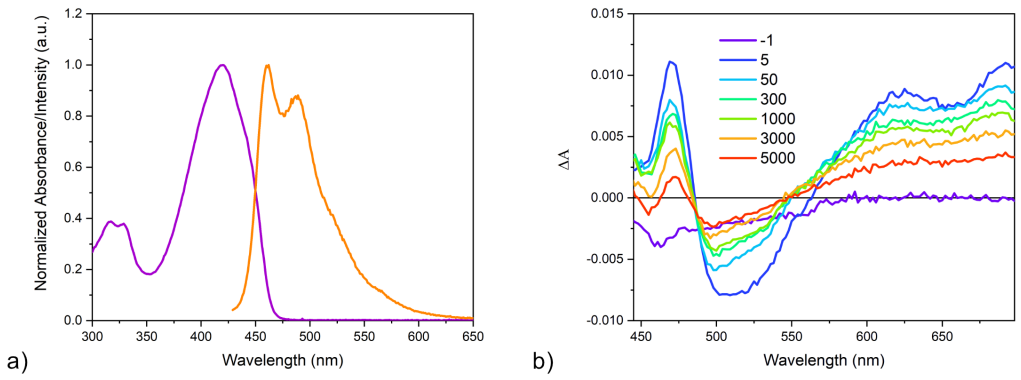

Figure 4.12: a) Steady state absorption and emission spectra of **DPIBF-C6** in toluene. b) fsTA spectra of **DPIBF-C6** in dilute solution. The fs measurements were performed in toluene with a pump pulse at 405 nm and the time delays presented in the legend are in ps.

The singlet has a sharp excited state absorption at ∼475 nm and a broader signal centered around 650 nm. The negative feature in between the two absorption bands is the stimulated emission which decays at the same rate as the ESA bands further reinforcing the assignment of the ESA bands to singlet excited state absorption.

The spectroscopic signature of the triplet excited state was obtained via triplet sensitization using **PtOEP** and the resulting spectra of the **DPIBF-C6** triplet is shown in Figure 4.13 with an absorption peak centered at 460 nm.

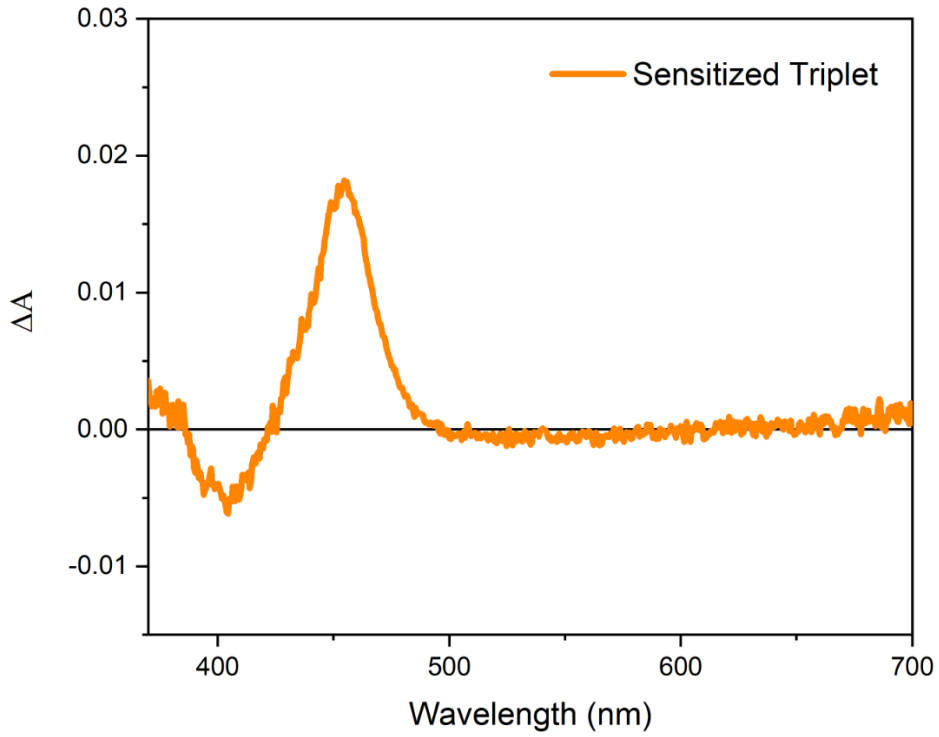

Figure 4.13: Sensitized triplet excited state spectra of **DPIBF-C6** obtained via triplet energy transfer from platinum octaethylporphyrin (**PtOEP**) in toluene solution.

Finally, the spectroscopic signature of the radical cation and anion are known from the literature for the parent molecule **DPIBF**. The radical cation have excited state absorption at ∼550 nm and the radical anion in turn have absorption at ∼650 nm.[69] Thus, if there is electron injection occurring the radical cation will be produced giving rise to absorption at 550 nm. Simultaneous absorption at 550 and 650 nm would imply that both the radical cation and anion are

present, i.e, that a charge separated state (CSS) has formed.

4.2.3 Photophysics of DPIBF-C6 attached to ZrO_2

As previously mentioned, ZrO_2 is used as a reference substrate where electron injection is substantially uphill in energy from both the singlet and triplet excited states of **DPIBF-C6**. Hence, on ZrO_2 SF and any competing processes can be investigated in absence of electron injection. The fsTA spectra of **DPIBF-C6** attached to ZrO_2 is presented in Figure 4.14 where 4.14a) shows the spectral evolution in acetonitrile (ϵ=37.5) and the results in 4.14b) were obtained in toluene (ϵ=2.38). In both solvents the initial spectra closely resembles the singlet excited state absorption that was observed when investigating the TA in solution. Here, however, the singlet excited state decays much more rapidly, which is in line with the observed heavily quenched fluorescence in Figure 4.11. The spectral evolution in the two solvents differs both from each other and from the sample in solution. For acetonitrile, absorption features centered around 550 and 650 nm start to appear when the singlet excited state absorption decays and these new absorption peaks match the spectra of the radical anion and cation. A weak absorption peak is also discernible at ~460 nm for later time delays which matches the triplet excited state. A similar, but slighly different spectral evolution is seen for toluene. In this case the absorption of the radical anion in particular is not very prominent and the triplet excited state absorption at 460 nm is stronger. These results taken together indicate that SF is occurring on ZrO_2 as evidenced by the triplet absorption. They also indicate that the SF is more efficient in toluene and that the reason may be that a CSS forms with roughly the same rate as the SF and thus acts loss channel to larger degree in a more polar environment. It should be mentioned that charge transfer states with spectroscopic signatures similar to a CCS state in certain systems have been proven to acts as intermediates for SF.[23,70,71] However, this does not appear to be the case here based on the parallel formation and decay of the CSS and the triplet in acetonitrile. The above assessment is also supported by estimations using equation 2.9 which places the charge separated state slightly above S_1 in toluene and slightly below in the more polar solvent acetonitrile.

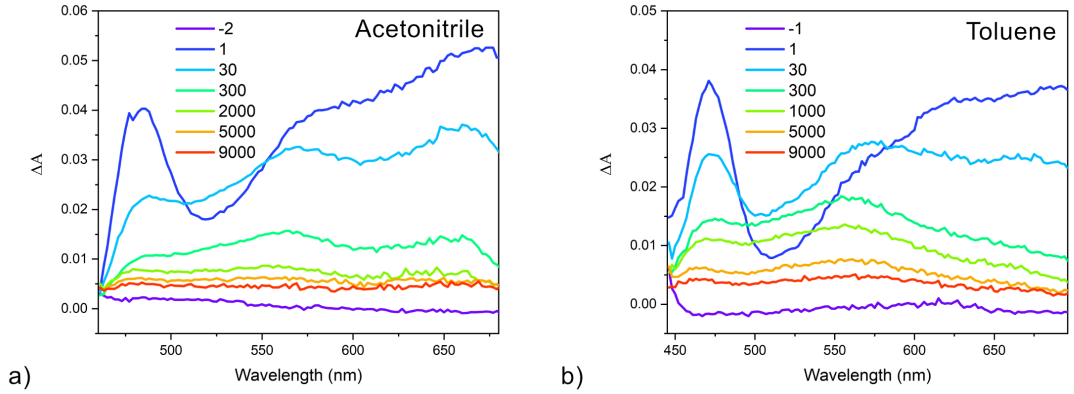

Figure 4.14: fsTA spectra of **DPIBF-C6** attached to ZrO_2 in a) acetonitrile and b) toluene using an excitation wavelength of 405 nm. The time delays presented in the legend are in ps.

These results indicate that the SF of **DPIBF-C6** attached to ZrO_2 is not very efficient even in toluene where the CSS is not a significant loss channel. This conclusion is based on the fairly weak triplet excited state absorption in both solvents. It should be noted that the triplet excited state has a slightly higher molar absorptivity than the singlet excited state, but even considering this the triplet signal can still be considered weak.[72] However, a fraction of the triplets that do form appear to have lifetimes exceeding 200 μs according to nsTA measurements. The nsTA spectra in Figure 4.15 also support the findings of the fsTA regarding that the triplet appears to be the specie with the longest lifetime.

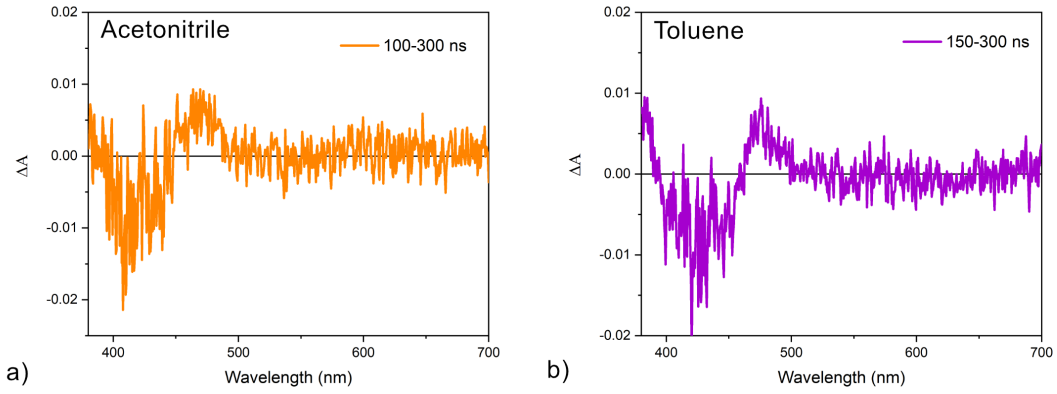

Figure 4.15: nsTA spectra of **DPIBF-C6** attached to ZrO_2 in a) acetonitrile and b) toluene using an excitation wavelength of 405 nm.

Furthermore, the relatively long lifetime of the triplet excited states indicate that the initially formed triplet pairs formed via intermolecular SF can dissociate into

free triplet states in contrast to what was seen in the study on the intramolecular SF of the dimers in section 4.1. This is reasonable since the triplet excited states can likely be transferred between different **DPIBF-C6** molecules in regions of short intermolecular distances between more than two molecules.

4.2.4 Photophysics of DPIBF-C6 attached to TiO_2

When **DPIBF-C6** is attached to TiO_2 both SF and electron injection from S_1 are possible processes and as such a competition of these is expected although the time resolved emission shown previously hints that electron injection may be the dominant process. Further insight into which process is favoured on the surface was obtained with fsTA and the result of the fsTA measurements of **DPIBF-C6** attached to TiO_2 immersed in acetonitrile or toluene are presented in Figure 4.16a) and b). As was the case for **DPIBF-C6** on ZrO_2 the spectra for the delay times immediately following excitation closely resemble the singlet excited state absorption. The dominating processes that occur subsequent to the decay of the singlet excited state are however distinctly different from those on ZrO_2 and so is the spectral evolution. In both solvents the singlet excited state signal decays rapidly and a new peak at 550 nm rises concomitantly with the decay of the singlet. This new absorption feature matches the spectra of the radical cation and since the radical anion signal at 650 nm is absent this is likely the result of efficient electron injection from the S_1 state into TiO_2. The fate of the CSS **DPIBF-C6**$^+$/$TiO_2(e^-)$ is however different for the two solvents as is made clear by their quite different spectral evolution at later time delays. In acetonitrile the polar environment stabilizes the CSS **DPIBF-C6**$^+$/$TiO_2(e^-)$ to some extent compared to in toluene resulting in a longer lifetime with only a marginal loss of the maximum signal strength at 9 ns. Interestingly, in toluene the radical cation signal decays much more rapidly and the decay is accompanied by a rise of the triplet excited state signal at 460 nm. Since the triplet excited state signal appears after the decay of the radical cation it is unlikely to be the result of SF. A more plausible explanation for the triplet formation could be that an alternative recombination pathway is available in toluene where the charge recombination from the CB of TiO_2 occurs to the triplet excited state of **DPIBF-C6** rather than the ground state.

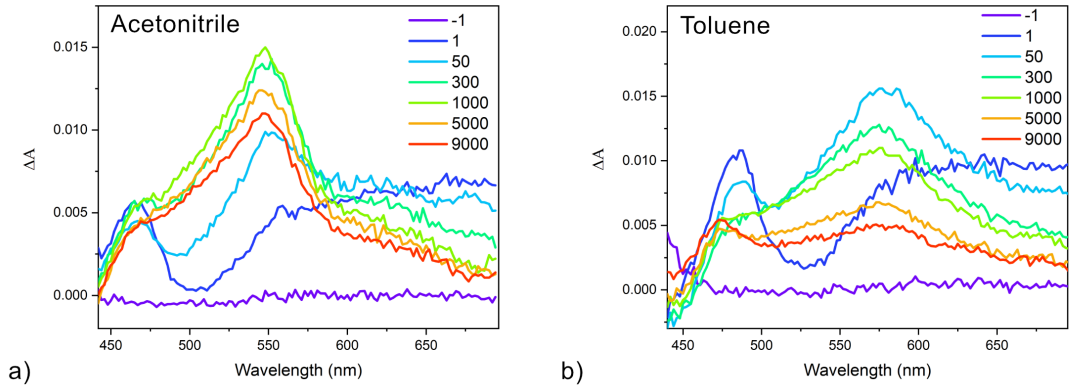

Figure 4.16: fsTA spectra of **DPIBF-C6** attached to TiO_2 in a) acetonitrile and b) toluene using an excitation wavelength of 405 nm. The time delays presented in the legend are in ps.

This hypothesis is supported by the nsTA measurements of **DPIBF-C6** on TiO_2 in both acetonitrile and toluene that are presented in Figure 4.17.

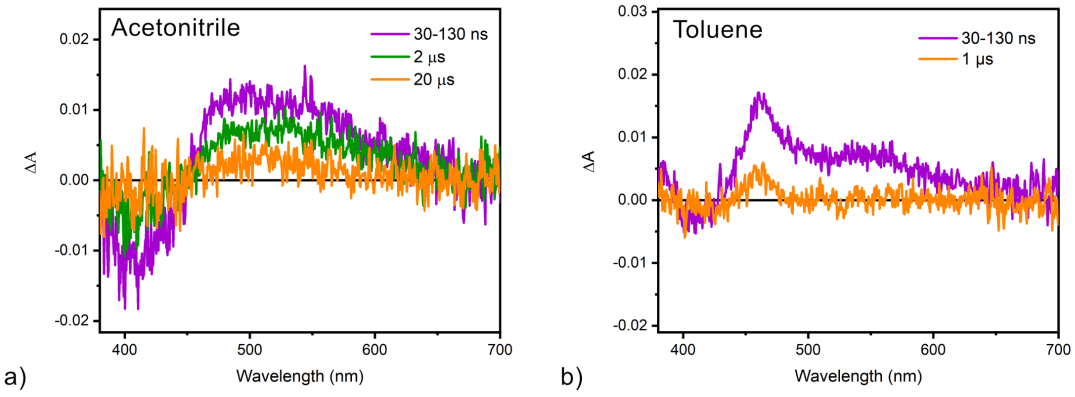

Figure 4.17: nsTA spectra of **DPIBF-C6** attached to TiO_2 in a) acetonitrile and b) toluene using an excitation wavelength of 405 nm.

In the case of acetonitrile the nsTA spectra is identical to the radical cation spectra in the fsTA measurements and the signal decays uniformly over the entire spectral range indicating recombination back to the ground state. In toluene the nsTA spectra initially resembles a mixture of the radical cation and the triplet excited state. At later times the radical cation has decayed completely while the triplet excited state remains, which further suggests that charge recombination occurs to the triplet excited state.

4.2.5 Photophysics of DPIBF-C6 attached to SnO_2

As shown in Figure 4.9 there is a substantial driving force for electron injection from both the triplet and singlet excited states for **DPIBF-C6** to SnO_2. Just as for ZrO_2 and TiO_2 the photophysics of **DPIBF-C6** bound to SnO_2 were investigated with TA and the fsTA in acetonitrile and toluene are shown in Figure 4.18. The spectra in both solvents initially look similar to what was observed for TiO_2 with singlet excited state absorption evolving into the radical cation signal as a result of electron injection from the singlet.

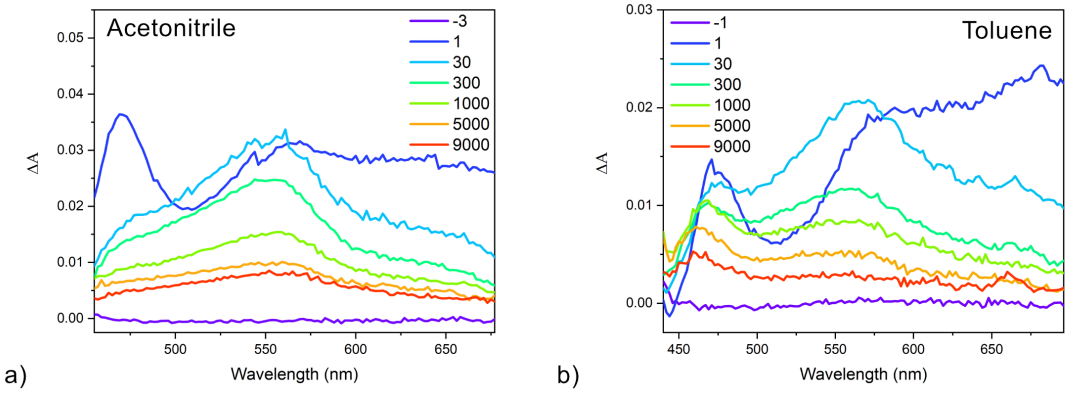

Figure 4.18: fsTA spectra of **DPIBF-C6** attached to SnO_2 in a) acetonitrile and b) toluene using an excitation wavelength of 405 nm. The time delays presented in the legend are in ps.

However, in the case of SnO_2 the radical cation signal is significantly less intense indicating that the electron injection yield is lower than for TiO_2 despite the larger driving force. The reason for this could be related to that the large driving force places the electron injection from the singlet in the inverted region. A closer inspection of the fsTA in the respective solvents reveals some interesting differences. In acetonitrile the only species that are discernible is the singlet that converts into the radical cation. For toluene there is an absorption peak that rises in the 460 nm region that matches the triplet excited state absorption. In this case there is no recombination pathway available from the CB of SnO_2 to the triplet and the triplets are thus likely formed via SF. It is somewhat unexpected that the SF appears to be more efficient on SnO_2 compared to on ZrO_2 considering that the SF in the case of SnO_2 also has to compete with electron injection from the singlet. A possible explanation for this observation could be

that the packing on the surface is different for the two semiconductors and that the self-assembly on SnO_2 is more favourable for SF.

Interestingly, the nsTA spectra of **DPIBF-C6** attached to SnO_2 shown in Figure 4.19 is remarkably similar for the two solvents with a broad feature resembling the spectra of the radical cation. This is not so surprising for acetonitrile since it is a continuation of the fsTA spectra and represent the recombination of the CSS **DPIBF-C6**$^+$/$SnO_2(e^-)$ on the microsecond timescale. In toluene, however, the spectra does not resemble the combination of the triplet excited state spectra and the radical cation as shown in the final time delay in the fsTA spectra in Figure 4.18b). Instead, the nsTA spectra is dominated by the radical cation spectroscopic signature indicating that the triplet excited state has decayed as a result of electron injection from the triplet.

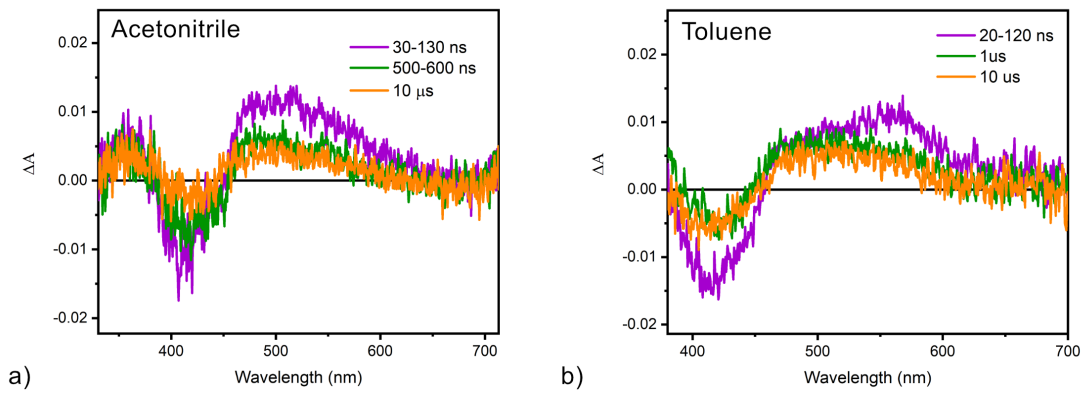

Figure 4.19: nsTA spectra of **DPIBF-C6** attached to SnO_2 in a) acetonitrile and b) toluene using an excitation wavelength of 405 nm.

4.2.6 Summary

In this section the characterization of the SF and electron injection capabilities of **DPIBF-C6** attached to several different mesoporous semiconductors in solvents of varying polarity has been presented. The study demonstrates how different processes can be favoured by altering the solvent polarity and by changing the driving force for electron injection. On ZrO_2 SF is most efficient in non-polar solvents which is at least partially a consequence of formation of a CSS in more polar solvents. On TiO_2 electron injection from the singlet excited state is the dominating process in both solvents. However, in non-polar solvents there is still

substantial triplet formation owing to charge recombination from the CB of TiO_2 rather than SF. Finally, on SnO_2 SF appears to occur in parallel with electron injection from S_1 and the formed triplet excited states are capable of electron injection.

As a final note it should be mentioned that most of the measurements presented above were also made with a derivative containing only five carbons (instead of six) in the alkane spacer. The ambition was in part to see if the shorter distance could have any effect on the ET rate from the singlet excited state. Furthermore, it was hypothesized that the spacer length could affect how the molecules were packed on the surface. This hypothesis was partly based on the fact that it has been proven that odd and even number of carbons in spacer groups of thiols attached to gold surfaces result in different kinds of packing and we speculated that this could be true also for the surface of the mesoporous semiconductors.[73] Unfortunately, we could observe no significant difference in the photophysics of the two derivatives and thus only the data from **DPIBF-C6** with six carbons in the spacer is presented herein.

5

Concluding Remarks and Future Work

In this thesis the main findings of **Paper I** and **Paper II** have been summarized. **Paper I** highlights the importance of considering the fact that molecules are not fully static systems and that a sample in solution at room temperature will contain molecules in a range of different conformations. Here, this has been utilized to design a SF system consisting of pentacene dimers in which a high viscosity environment allows for both efficient SF and long triplet lifetimes in the same system. Furthermore, we have shown that it is possible to selectively excite different rotational conformations of the dimers at cryogenic temperatures. The different conformations display orders of magnitude different SF rate depending on which wavelength they are excited with and this is most likely directly connected to the amount of conjugation and orbital overlap of the conformation that is initially photoexcited.

The study on mesoporous semiconductors in combination with the SF molecule DPIBF-C6 bound to the surface in **Paper II** have revealed several challenges associated with integrating a SF material with semiconductors. In summary, we have found that the rate of both SF and electron injection are heavily dependent on the surrounding environment in terms of the self-assembly on the surface, electron injection driving force and solvent polarity. The study has shown that it is beneficial to use a semiconductor with a low CB edge in combination with a non-polar solvent for optimal harvesting of the generated triplet excitons from SF. The non-polar solvent is necessary to avoid the formation of stable CSSs that can outcompete the SF. Unexpectedly, SF was found to be more efficient on SnO_2 than on ZrO_2 despite the competition with electron injection from the

singlet state in the former case. The reasons behind this are currently not clear but could be related to slightly different nanoparticle networks that affects how DPIBF-C6 is attached to the surface and which in turn affects the packing and orientation of the DPIBF-C6 molecules relative to each other. Better control of the distance and electronic coupling between SF molecules on the surface could potentially be solved by instead attaching dimers to the surface and hence rely on intramolecular rather than intermolecular SF. In a dimer such as the one's studied in **Paper I** the SF moieties are already in fairly well-defined orientations and could be interesting to study in combination with semiconductor acceptors in future studies.

Additional avenues that should be explored would be to use organic molecules rather than semiconductors as electron acceptors. SF has the potential to overcome some of the problems associated with photoredox reactions since they in many cases require multiple electrons to proceed. This generally requires absorption of multiple photons since one photon typically only gives rise to one exciton. Additionally, the intermediates that are formed are often highly reactive leading to unwanted side reactions. Since SF produces two excitons for each incident photon it has the potential to enable such reduction reactions since both electrons in theory could be transferred in very close succession. There are also many examples of molecules where the reduction potential is much more accessible for two electrons rather than one. One such example is the reduction of CO_2 for which the single electron reduction is -1.9 V vs. NHE and the 2-electron reduction is only -0.53 V vs. NHE.[74] The potential for SF in multielectron redox chemistry is largely unexplored in the literature and our future work will seek to use the knowledge gained herein regarding how to design dimers with efficient SF in combination with long triplet lifetimes and apply this to multielectron photocatalysis.

6

Acknowledgements

There are many people that I would like to express my gratitude towards and I will start with my supervisor Bo Albinsson. Thank you for recruiting me and allowing me to work on such fascinating projects. Your guidance and continuous help throughout my time as a PhD-student has made me grow not only as a scientist, but as a person as well.

A huge thank you also to my co-supervisor Maria Abrahamsson for your support and guidance. Without you I would likely never have gotten into this intriguing field of research. I am also thankful to my examiner Joakim Andréasson for always providing help when needed.

Thank you both past and present members of the Albinsson, Abrahamsson, Andréasson research groups and all the people at the department in general for your positive attitudes, interesting scientific discussions and for always being helpful in the lab. A special thank you to Fredrik Edhborg for our work together on shared projects and for always being happy to answer any question I have. You have taught me so much and I am very grateful for all the fun we have had in the lab together. Thank you also to Elin Sundin and Betül Küçüköz for our work together and for having the patience to teach a young little master's student in the ways of spectroscopy. And my office mates Liam Mistry and Andrew Maurer - thank you so much for all your help and interesting discussions and for creating a wonderful work atmosphere.

Finally, I want to acknowledge all the support I have received from my friends, family and extended family. A special thanks goes to my parents Bo and Gisela, and my sister Hannah. I want to thank you not only for always being supportive

in my doctoral studies, but also for all the guidance and help I have received over the years and for being the best family I could ever imagine having. Lastly, I want to thank Wilma for always being there for me and for making me the happiest I have ever been. I love you all very much.

Bibliography

[1] J. Perlin. *From space to earth: the story of solar electricity*. Aatec Publications, Ann Arbor, Mich, 1999.

[2] D. Feldman, V. Ramasamy, R. Fu, A. Ramdas, J. Desai, and R. Margolis. U.S. Solar Photovoltaic System and Energy Storage Cost Benchmark: Q1 2020, 2021. NREL/TP-6A20-77324.

[3] W. Bludau, A. Onton, and W. Heinke. Temperature dependence of the band gap of silicon. *Journal of Applied Physics*, 45(4):1846–1848, April 1974.

[4] M. Woodhouse, R. Jones-Albertus, D. Feldman, R. Fu, K. Horowitz, D. Chung, D. Jordan, and S. Kurtz. On the Path to SunShot: The Role of Advancements in Solar Photovoltaic Efficiency, Reliability, and Costs, 2016. NREL/TP-6A20-65872.

[5] W. Shockley and H. J. Queisser. Detailed Balance Limit of Efficiency of *p-n* Junction Solar Cells. *Journal of Applied Physics*, 32(3):510–519, March 1961.

[6] National Renewable Energy Laboratory, Reference air mass 1.5 spectra. https://www.nrel.gov/grid/solar-resource/spectra-am1.5.html. Accessed: 2022-06-29.

[7] M. B. Smith and J. Michl. Singlet Fission. *Chemical Reviews*, 110(11):6891–6936, November 2010.

[8] J. Lee, P. Jadhav, P. D. Reusswig, S. R. Yost, N. J. Thompson, D. N. Congreve, E. Hontz, T. Van Voorhis, and M. A. Baldo. Singlet Exciton Fission Photovoltaics. *Accounts of Chemical Research*, 46(6):1300–1311, June 2013.

[9] M. C. Hanna and A. J. Nozik. Solar conversion efficiency of photovoltaic and photoelectrolysis cells with carrier multiplication absorbers. *Journal of Applied Physics*, 100(7):074510, October 2006.

[10] S. Dahl and I. Chorkendorff. Towards practical implementation. *Nature Materials*, 11(2):100–101, February 2012.

[11] P. W. Atkins and R. Friedman. *Molecular quantum mechanics*. Oxford University Press, Oxford ; New York, 5th ed edition, 2011.

[12] J. M. Hollas. *Modern spectroscopy*. J. Wiley, Chichester ; Hoboken, NJ, 4th ed edition, 2004.

[13] P. W. Atkins, J. De Paula, and R. Friedman. *Physical chemistry: quanta, matter, and change*. Oxford University Press, Oxford, United Kingdom, second edition edition, 2014. OCLC: ocn870161002.

[14] M. Montalti, A. Credi, L. Prodi, and M. T. Gandolfi. *Handbook of Photochemistry*. CRC Press, 0 edition, February 2006.

[15] C. Schweitzer and R. Schmidt. Physical Mechanisms of Generation and Deactivation of Singlet Oxygen. *Chemical Reviews*, 103(5):1685–1758, May 2003.

[16] W. T. Silfvast. *Laser Fundamentals*. Cambridge University Press, 2 edition, January 2004.

[17] M. Kasha. Characterization of electronic transitions in complex molecules. *Discussions of the Faraday Society*, 9:14, 1950.

[18] D. L. Dexter. A Theory of Sensitized Luminescence in Solids. *The Journal of Chemical Physics*, 21(5):836–850, May 1953.

[19] T. Főrster. 10th Spiers Memorial Lecture. Transfer mechanisms of electronic excitation. *Discuss. Faraday Soc.*, 27(0):7–17, 1959.

[20] J. R. Lakowicz. *Principles of fluorescence spectroscopy*. Springer, New York, 3rd ed edition, 2006.

[21] M. B. Smith and J. Michl. Recent Advances in Singlet Fission. *Annual Review of Physical Chemistry*, 64(1):361–386, April 2013.

[22] B. J. Walker, A. J. Musser, D. Beljonne, and R. H. Friend. Singlet exciton fission in solution. *Nature Chemistry*, 5(12):1019–1024, December 2013.

[23] M. Chen, Y. J. Bae, C. M. Mauck, A. Mandal, R. M. Young, and M. R. Wasielewski. Singlet Fission in Covalent Terrylenediimide Dimers: Probing the Nature of the Multiexciton State Using Femtosecond Mid-Infrared Spectroscopy. *Journal of the American Chemical Society*, 140(29):9184–9192, July 2018.

[24] B. S. Basel, J. Zirzlmeier, C. Hetzer, B. T. Phelan, M. D. Krzyaniak, S. R. Reddy, P. B. Coto, N. E. Horwitz, R. M. Young, F. J. White, F. Hampel, T. Clark, M. Thoss, R. R. Tykwinski, M. R. Wasielewski, and D. M. Guldi. Unified model for singlet fission within a non-conjugated covalent pentacene dimer. *Nature Communications*, 8(1):15171, August 2017.

[25] J. Zirzlmeier, D. Lehnherr, P. B. Coto, E. T. Chernick, R. Casillas, B. S. Basel, M. Thoss, R. R. Tykwinski, and D. M. Guldi. Singlet fission in pentacene dimers. *Proceedings of the National Academy of Sciences*, 112(17):5325–5330, April 2015.

[26] S. N. Sanders, E. Kumarasamy, A. B. Pun, M. T. Trinh, B. Choi, J. Xia, E. J. Taffet, J. Z. Low, J. R. Miller, X. Roy, X.-Y. Zhu, M. L. Steigerwald, M. Y. Sfeir, and L. M. Campos. Quantitative Intramolecular Singlet Fission in Bipentacenes. *Journal of the American Chemical Society*, 137(28):8965–8972, July 2015.

[27] B. S. Basel, J. Zirzlmeier, C. Hetzer, S. R. Reddy, B. T. Phelan, M. D. Krzyaniak, M. K. Volland, P. B. Coto, R. M. Young, T. Clark, M. Thoss, R. R. Tykwinski, M. R. Wasielewski, and D. M. Guldi. Evidence for Charge-Transfer Mediation in the Primary Events of Singlet Fission in a Weakly Coupled Pentacene Dimer. *Chem*, 4(5):1092–1111, May 2018.

[28] H. Liu, Z. Wang, X. Wang, L. Shen, C. Zhang, M. Xiao, and X. Li. Singlet exciton fission in a linear tetracene tetramer. *Journal of Materials Chemistry C*, 6(13):3245–3253, 2018.

[29] A. M. Müller, Y. S. Avlasevich, W. W. Schoeller, K. Müllen, and C. J. Bardeen. Exciton Fission and Fusion in Bis(tetracene) Molecules with Different Covalent Linker Structures. *Journal of the American Chemical Society*, 129(46):14240–14250, November 2007.

[30] N. V. Korovina, J. Joy, X. Feng, C. Feltenberger, A. I. Krylov, S. E. Bradforth, and M. E. Thompson. Linker-Dependent Singlet Fission in Tetracene Dimers. *Journal of the American Chemical Society*, 140(32):10179–10190, August 2018.

[31] I. Papadopoulos, J. Zirzlmeier, C. Hetzer, Y. J. Bae, M. D. Krzyaniak, M. R. Wasielewski, T. Clark, R. R. Tykwinski, and D. M. Guldi. Varying the Interpentacene Electronic Coupling to Tune Singlet Fission. *Journal of the American Chemical Society*, 141(15):6191–6203, April 2019.

[32] S. Lukman, K. Chen, J. M. Hodgkiss, D. H. P. Turban, N. D. M. Hine, S. Dong, J. Wu, N. C. Greenham, and A. J. Musser. Tuning the role of charge-transfer states in intramolecular singlet exciton fission through side-group engineering. *Nature Communications*, 7(1):13622, December 2016.

[33] J. C. Johnson and J. Michl. 1,3-Diphenylisobenzofuran: a Model Chromophore for Singlet Fission. *Topics in Current Chemistry*, 375(5):80, October 2017.

[34] J. C. Johnson, A. J. Nozik, and J. Michl. High Triplet Yield from Singlet Fission in a Thin Film of 1,3-Diphenylisobenzofuran. *Journal of the American Chemical Society*, 132(46):16302–16303, November 2010.

[35] A. Akdag, A. Wahab, P. Beran, L. Rulíšek, P. I. Dron, J. Ludvík, and J. Michl. Covalent Dimers of 1,3-Diphenylisobenzofuran for Singlet Fission: Synthesis and Electrochemistry. *The Journal of Organic Chemistry*, 80(1):80–89, January 2015.

[36] S. W. Eaton, L. E. Shoer, S. D. Karlen, S. M. Dyar, E. A. Margulies, B. S. Veldkamp, C. Ramanan, D. A. Hartzler, S. Savikhin, T. J. Marks, and M. R. Wasielewski. Singlet Exciton Fission in Polycrystalline Thin Films of a Slip-Stacked Perylenediimide. *Journal of the American Chemical Society*, 135(39):14701–14712, October 2013.

[37] M. Chen, N. E. Powers-Riggs, A. F. Coleman, R. M. Young, and M. R. Wasielewski. Singlet Fission in Quaterrylenediimide Thin Films. *The Journal of Physical Chemistry C*, 124(5):2791–2798, February 2020.

[38] M. Dvořák, S. K. K. Prasad, C. B. Dover, C. R. Forest, A. Kaleem, R. W. MacQueen, A. J. Petty, R. Forecast, J. E. Beves, J. E. Anthony, M. J. Y. Tayebjee, A. Widmer-Cooper, P. Thordarson, and T. W. Schmidt. Singlet Fission in Concentrated TIPS-Pentacene Solutions: The Role of Excimers and Aggregates. *Journal of the American Chemical Society*, 143(34):13749–13758, September 2021.

[39] J. R. Allardice, A. Thampi, S. Dowland, J. Xiao, V. Gray, Z. Zhang, P. Budden, A. J. Petty, N. J. L. K. Davis, N. C. Greenham, J. E. Anthony, and A. Rao. Engineering Molecular Ligand Shells on Quantum Dots for Quantitative Harvesting of Triplet Excitons Generated by Singlet Fission. *Journal of the American Chemical Society*, 141(32):12907–12915, August 2019.

[40] R. A. Marcus. Electron Transfer Reactions in Chemistry: Theory and Experiment (Nobel Lecture). *Angewandte Chemie International Edition in English*, 32(8):1111–1121, August 1993.

[41] J. R. Bolton, N. Mataga, and G. McLendon, editors. *Electron Transfer in Inorganic, Organic, and Biological Systems*, volume 228 of *Advances in Chemistry*. American Chemical Society, Washington, DC, May 1991.

[42] M. R. Wasielewski. Photoinduced electron transfer in supramolecular systems for artificial photosynthesis. *Chemical Reviews*, 92(3):435–461, May 1992.

[43] R. Marcus and N. Sutin. Electron transfers in chemistry and biology. *Biochimica et Biophysica Acta (BBA) - Reviews on Bioenergetics*, 811(3):265–322, August 1985.

[44] E. Vauthey. Photoinduced Symmetry-Breaking Charge Separation. *ChemPhysChem*, 13(8):2001–2011, June 2012.

[45] P. F. Barbara, T. J. Meyer, and M. A. Ratner. Contemporary Issues in Electron Transfer Research. *The Journal of Physical Chemistry*, 100(31):13148–13168, January 1996.

[46] A. Weller. Photoinduced Electron Transfer in Solution: Exciplex and Radical Ion Pair Formation Free Enthalpies and their Solvent Dependence. *Zeitschrift für Physikalische Chemie*, 133(1):93–98, January 1982.

[47] K. Kilså, A. N. Macpherson, T. Gillbro, J. Mårtensson, and B. Albinsson. Control of electron transfer in supramolecular systems. *Spectrochimica Acta Part A: Molecular and Biomolecular Spectroscopy*, 57(11):2213–2227, September 2001.

[48] D. R. Askeland and W. J. Wright. *The science and engineering of materials*. Cengage Learning, Boston, MA, seventh edition edition, 2016. OCLC: ocn903959750.

[49] A. Brodeur and S. L. Chin. Ultrafast white-light continuum generation and self-focusing in transparent condensed media. *Journal of the Optical Society of America B*, 16(4):637, April 1999.

[50] D. V. O'Connor and D. Phillips. *Time-correlated single photon counting*. Academic Press, London ; Orlando, 1984.

[51] I. H. van Stokkum, D. S. Larsen, and R. van Grondelle. Global and target analysis of time-resolved spectra. *Biochimica et Biophysica Acta (BBA) -*

Bioenergetics, 1657(2-3):82–104, July 2004.

[52] C. Ruckebusch, M. Sliwa, P. Pernot, A. de Juan, and R. Tauler. Comprehensive data analysis of femtosecond transient absorption spectra: A review. *Journal of Photochemistry and Photobiology C: Photochemistry Reviews*, 13(1):1–27, March 2012.

[53] R. W. Hendler and R. I. Shrager. Deconvolutions based on singular value decomposition and the pseudoinverse: a guide for beginners. *Journal of Biochemical and Biophysical Methods*, 28(1):1–33, January 1994.

[54] J. M. Beechem. [2] Global analysis of biochemical and biophysical data. In *Methods in Enzymology*, volume 210, pages 37–54. Elsevier, 1992.

[55] H. Satzger and W. Zinth. Visualization of transient absorption dynamics – towards a qualitative view of complex reaction kinetics. *Chemical Physics*, 295(3):287–295, December 2003.

[56] R. Ringström, F. Edhborg, Z. W. Schroeder, L. Chen, M. J. Ferguson, R. R. Tykwinski, and B. Albinsson. Molecular rotational conformation controls the rate of singlet fission and triplet decay in pentacene dimers. *Chemical Science*, 13(17):4944–4954, 2022.

[57] M. Mizukami, H. Fujimori, and M. Oguni. Glass Transitions and the Responsible Molecular Motions in 2-Methyltetrahydrofuran. *Progress of Theoretical Physics Supplement*, 126(0):79–82, May 2013.

[58] E. Sundin, R. Ringström, F. Johansson, B. Küçüköz, A. Ekebergh, V. Gray, B. Albinsson, J. Mårtensson, and M. Abrahamsson. Singlet Fission and Electron Injection from the Triplet Excited State in Diphenylisobenzofuran–Semiconductor Assemblies: Effects of Solvent Polarity and Driving Force. *The Journal of Physical Chemistry C*, 124(38):20794–20805, September 2020.

[59] F. Ambrosio, N. Martsinovich, and A. Troisi. What Is the Best Anchoring Group for a Dye in a Dye-Sensitized Solar Cell? *The Journal of Physical Chemistry Letters*, 3(11):1531–1535, June 2012.

[60] T. Banerjee, S. P. Hill, M. A. Hermosilla-Palacios, B. D. Piercy, J. Haney, B. Casale, A. E. DePrince, M. D. Losego, V. D. Kleiman, and K. Hanson. Diphenylisobenzofuran Bound to Nanocrystalline Metal Oxides: Excimer Formation, Singlet Fission, Electron Injection, and Low Energy Sensitiza-

tion. *The Journal of Physical Chemistry C*, 122(50):28478–28490, December 2018.

[61] S. P. Hill, T. Banerjee, T. Dilbeck, and K. Hanson. Photon Upconversion and Photocurrent Generation via Self-Assembly at Organic–Inorganic Interfaces. *The Journal of Physical Chemistry Letters*, 6(22):4510–4517, November 2015.

[62] R. L. Milot, G. F. Moore, R. H. Crabtree, G. W. Brudvig, and C. A. Schmuttenmaer. Electron Injection Dynamics from Photoexcited Porphyrin Dyes into SnO_2 and TiO_2 Nanoparticles. *The Journal of Physical Chemistry C*, 117(42):21662–21670, October 2013.

[63] R. Katoh, A. Furube, T. Yoshihara, K. Hara, G. Fujihashi, S. Takano, S. Murata, H. Arakawa, and M. Tachiya. Efficiencies of Electron Injection from Excited N3 Dye into Nanocrystalline Semiconductor (ZrO_2, TiO_2, ZnO, Nb_2O_5, SnO_2, In_2O_3) Films. *The Journal of Physical Chemistry B*, 108(15):4818–4822, April 2004.

[64] R. W. Fessenden and P. V. Kamat. Rate Constants for Charge Injection from Excited Sensitizer into SnO2, ZnO, and TiO2 Semiconductor Nanocrystallites. *The Journal of Physical Chemistry*, 99(34):12902–12906, August 1995.

[65] M. A. Butler and D. S. Ginley. Prediction of Flatband Potentials at Semiconductor-Electrolyte Interfaces from Atomic Electronegativities. *Journal of The Electrochemical Society*, 125(2):228–232, February 1978.

[66] Y. Tachibana, J. E. Moser, M. Grätzel, D. R. Klug, and J. R. Durrant. Subpicosecond Interfacial Charge Separation in Dye-Sensitized Nanocrystalline Titanium Dioxide Films. *The Journal of Physical Chemistry*, 100(51):20056–20062, January 1996.

[67] D. Cahen, G. Hodes, M. Grätzel, J. F. Guillemoles, and I. Riess. Nature of Photovoltaic Action in Dye-Sensitized Solar Cells. *The Journal of Physical Chemistry B*, 104(9):2053–2059, March 2000.

[68] N. A. Pace, D. H. Arias, D. B. Granger, S. Christensen, J. E. Anthony, and J. C. Johnson. Dynamics of singlet fission and electron injection in self-assembled acene monolayers on titanium dioxide. *Chemical Science*, 9(11):3004–3013, 2018.

[69] A. F. Schwerin, J. C. Johnson, M. B. Smith, P. Sreearunothai, D. Popović, J. Černý, Z. Havlas, I. Paci, A. Akdag, M. K. MacLeod, X. Chen, D. E. David, M. A. Ratner, J. R. Miller, A. J. Nozik, and J. Michl. Toward Designed Singlet Fission: Electronic States and Photophysics of 1,3-Diphenylisobenzofuran. *The Journal of Physical Chemistry A*, 114(3):1457–1473, January 2010.

[70] R. M. Young and M. R. Wasielewski. Mixed Electronic States in Molecular Dimers: Connecting Singlet Fission, Excimer Formation, and Symmetry-Breaking Charge Transfer. *Accounts of Chemical Research*, 53(9):1957–1968, September 2020.

[71] N. Monahan and X.-Y. Zhu. Charge Transfer–Mediated Singlet Fission. *Annual Review of Physical Chemistry*, 66(1):601–618, April 2015.

[72] J. N. Schrauben, J. L. Ryerson, J. Michl, and J. C. Johnson. Mechanism of Singlet Fission in Thin Films of 1,3-Diphenylisobenzofuran. *Journal of the American Chemical Society*, 136(20):7363–7373, May 2014.

[73] L. Ramin and A. Jabbarzadeh. Odd–Even Effects on the Structure, Stability, and Phase Transition of Alkanethiol Self-Assembled Monolayers. *Langmuir*, 27(16):9748–9759, August 2011.

[74] E. E. Benson, C. P. Kubiak, A. J. Sathrum, and J. M. Smieja. Electrocatalytic and homogeneous approaches to conversion of CO_2 to liquid fuels. *Chem. Soc. Rev.*, 38(1):89–99, 2009.